Using Isothermal Titration Calorimetry to Characterize the Ca^{2+} Binding Properties of Cardiac Troponin C and Slow Skeletal-specific Troponin C in Zebrafish

by

Cindy Li

B.Sc., Simon Fraser University, 2009

Thesis Submitted in Partial Fulfillment of the
Requirements for the Degree of
Master of Science

in the
Department of Molecular Biology and Biochemistry
Faculty of Science

SIMON FRASER UNIVERSITY

Spring 2014

Approval

Name: **Cindy Li**

Degree: **Master of Science (Molecular Biology and Biochemistry)**

Title of Thesis: ***Using Isothermal Titration Calorimetry to Characterize the Ca^{2+} Binding Properties of Cardiac Troponin C and Slow Skeletal-specific Troponin C in Zebrafish***

Examining Committee: **Chair:** Nancy Hawkins
Associate Professor, MBB

Dr. Glen Tibbits
Senior Supervisor
Professor, BPK

Dr. Edgar Young
Supervisor
Associate Professor, MBB

Dr. Jonathan Choy
Supervisor
Assistant Professor, MBB

Dr. Filip Van Petegem
Supervisor
Associate Professor, Biochemistry and Molecular Biology (UBC)

Dr. Thomas Claydon
Internal Examiner
Associate Professor, BPK

Date Defended/Approved: April 16th, 2014

Partial Copyright Licence

Abstract

Slow skeletal-specific TnC (ssTnC, *tnnc1b*), found only in teleosts, and cardiac troponin C (cTnC, *tnnc1a*) are both expressed in zebrafish (ZF) heart in a temperature- and chamber-specific pattern. The focus of this study is to determine the Ca^{2+} binding affinities (K_{Ca}) of the regulatory site in ZF cTnC and ssTnC, and the thermal stability of each protein. Isothermal titration calorimetry was used to determine the K_{Ca} of the N-terminal domain of ZF cTnC and ssTnC at 8°C, 18°C and 28°C. The results for both TnCs show an increase in K_{Ca} with increasing temperature. The melting temperature (T_m) of each protein was also determined from thermal melting curves. The results show that ZF cTnC is slightly more stable with a T_m of 2°C higher. The data obtained provide functional insight into the Ca^{2+} binding properties of ZF TnC. It also provides a better understanding of teleost TnC sub-functionalization for chamber-specific expression seen in ZF.

Keywords: troponin C; zebrafish; isothermal titration calorimetry; Ca^{2+} binding affinity; melting temperature

To my family and friends.

Acknowledgements

I would like to thank Dr. Glen Tibbits for taking me in as a member of the cardiac troponin group. I am also thankful for the funding he has provided, which allowed me to conduct research full-time and for the opportunities he has provided me for attending conferences.

I would also like to thank Dr. Edgar Young, Dr. Jonathan Choy and Dr. Filip Van Petegem for being on my supervisory committee. Their input and suggestions over the years are greatly appreciated. I would also like to thank Dr. Thomas Claydon and Dr. Nancy Hawkins for agreeing to serve as my Internal and Chair for my defence.

I would also like to thank Dr. Filip Van Petegem for his time in answering questions and his invaluable input towards the project. I would also like to thank members of the Van Petegem lab: Kelvin Lau, Paolo Lobo, Jett Tung, Siobhan Wong, Michael Yuchi, Bernd Gardill and Samir Das. Their effort and time in training me to use their instruments helped made this project possible.

I would like to thank Dr. Charles Stevens and Alison Li from the Tibbits lab for their support over the years and for their help in editing this thesis. I would also like to thank Bo Liang, Christine Genge, and Laura Dewar for their support and help over the years.

I would also like to thank previous and existing members of the Paetzel lab: Dr. Mark Paetzel, Deidre de Jong-Wong, Dr. David Oliver, Dr. Jae-Yong Lee, Dr. Sung-Eun Nam, Dr. Charles Stevens, Dr. Apollos Kim, Dr. Ivy Chung, Daniel Chiang, Linda Zhang, Suraaj Aulakh, Yun Luo, and Alison Li for the training I received during my ISS.

I would also like to thank Dr. Nancy Forde and Andrew Wieczorek for their support, advice and encouragement over the years. The training I previously received in the Forde Lab is also deeply appreciated.

Finally, I would like to thank my family and friends for their continuous support and encouragement over the years.

Table of Contents

List of Tables

List of Figures

List of Acronyms

cTn	cardiac troponin
cTnC	cardiac troponin C
cTnI	cardiac troponin I
cTnT	cardiac troponin T
DCM	dilated cardiomyopathy
EST	expressed sequence tag
fsTnC	fast skeletal troponin C
HCM	hypertrophic cardiomyopathy
IAANS	2-4(4'-(iodoacetamido)aniline)-naphthalene-6-sulfonic acid
IAEDANS	5-((2-[iodoacetyl)amino]ethyl)amino)naphalene-1-sulfonic acid
IANBD	N-(2-(iodoacteoxy)ethyl)-N-methyl-amino-7-mitrobenz-2-oxa-1,3-diazole)
ITC	isothermal titration calorimetry
K_a	binding affinity (unit: per molar)
K_d	dissociation constant (unit: molar or micromolar)
kDa	kiloDalton (unit for molecular mass; 1 kiloDalton = 1000 Daltons)
mAu	milli-absorbance unit
N	molar ratio
NMR	nuclear magnetic resonance
NTnC	N-terminal domain of troponin C (residues 1 to 89)
PDB	Protein Data Bank (database of 3D coordinates of known protein structures)
RCM	restricted cardiomyopathy
SDS-PAGE	sodium dodecyl sulphate polyacrylamide gel electrophoresis
SR	sarcoplasmic reticulum
ssNTnC	slow skeletal-specific N-terminal domain of troponin C (residues 1 to 89)
T_m	melting temperature
Tn	troponin
WT	wild-type
ZF	zebrafish
ΔG	change in Gibb's free energy (unit: calories per mole)

ΔH	change in enthalpy (unit: calories per mole)
ΔS	change in entropy (unit: calories per mole per degree Kelvin)

Chapter 1. Introduction

1.1. Brief background to teleost heart anatomy

Teleost hearts are designed for the optimal delivery of oxygen to working skeletal muscle and systemic tissues in an oxygen poor environment. The teleost heart contains four chambers: the sinus venosus, atrium, ventricle and bulbus arteriosus (Figure 1.1.1). The atrium and ventricle serve as pumps to regulate blood flow. Circulation of blood occurs in a serial pattern where oxygen is exchanged at the gills and blood flows through the body until it reaches the sinus venosus as a de-oxygenated blood. In contrast, vertebrate species have developed hearts with multiple chambers that allow for the delivery of oxygenated and deoxygenated blood in a parallel pattern. With this development the left ventricle can generate larger forces and pressures (Moorman and Christoffels 2003).

The sinus venosus is a non-pumping chamber and developed as a separate compartment with low muscle content of the fish heart. It serves as a drainage pool of the venous system and aids in atrial filling. The teleost atrium, unlike those in mammalian species, is the principle driving force for ventricular filling. Generally, the teleost atrium has a similar volume as that of its ventricles. The size and volume of teleost atria indicate the importance of atrial function as the principle force for ventricular filling. In contrast, the right atrium in mammalian species has evolved from the teleost sinus venous and tends to be smaller in volume in comparison to the volume of ventricles. The mammalian atria's main function is in the collection of blood although atrial contraction is thought to contribute to about 20% of ventricular filling and this value increases during exercise (Moorman and Christoffels 2003).

Blood is ejected from the ventricle into the bulbus arteriosus. The ventricle has a mass and wall-thickness that is five-times higher than that of the atrium. This reflects the chamber's function as the active determinant of cardiac output. The bulbous arteriosus is

made of elastic tissue and smooth muscle. At the embryonic stage, the bulbous arteriosus is surrounded by myocardium but disappears with development. The high compliance of the chamber serves to dampen the pulsatility of the blood ejected from the ventricle thereby protecting the gill vasculature (Moorman and Christoffels 2003, Icardo 2012).

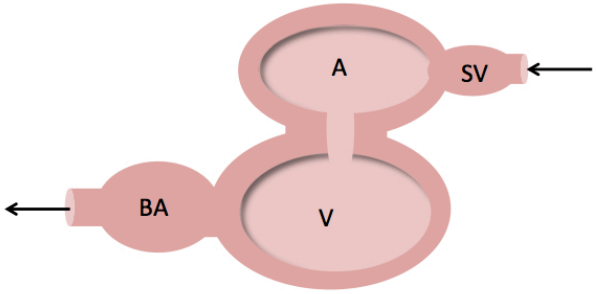

Figure 1.1.1 Cartoon image of the teleost heart.
Cartoon image of telesot heart where SV is the sinus venous, A is atrium, V is ventricle and BA is bulbus arteriosus. Arrows indicate the direction of blood flow.

1.2. Excitation-contraction coupling in mammalian and teleost cardiomyocytes

Transverse tubules (T-tubules) in mammalian cardiomyocytes are invaginations of the cell membrane and serve as important sites for excitation-contraction coupling (E-C coupling). E-C coupling refers to the process of muscle cell excitation causing the influx of ions across the cell-membrane that leads to contraction. T-tubules have a periodicity of about 2 µm, are aligned with the Z discs and lie in close proximity to the junctional sarcoplasmic reticulum (SR) where ryanodine receptors are located. L-type calcium channels ($Ca_V1.2$) are dispersed throughout the T-tubule structures found in adult mammalian cardiomyocytes and play an important role for the influx of Ca^{2+} during E-C coupling (Bers 2002). When L-type calcium channels are activated via excitation of the cell membrane, there is an influx of Ca^{2+}. As cytosolic Ca^{2+} concentration increases, Ca^{2+} binds to ryanodine receptors of which in turn release the stored Ca^{2+} within the SR into the cytosol. The increase of Ca^{2+} leads to binding of Ca^{2+} to cardiac troponin C

(cTnC) and as a result, leads to muscle contraction (Bodi, Mikala et al. 2005, Van Petegem 2012).

Adult teleost cardiomyocytes lack T-tubules, resemble mammalian neonatal cardiomyocytes in many respects and have a long (>100 μm in length) yet thinner shape (<10 μm in width) than those observed in mammalian cardiomyocytes. (Vornanen 1997, Vornanen 1998, Huang, Hove-Madsen et al. 2005). It is speculated that the reduced diameter of teleost cardiomyocytes contributes to the decrease in diffusion rate for ions and therefore increases the efficiency for E-C coupling (Di Maio and Block 2008, Genge, Davidson et al. 2013). In addition to the lack of T-tubules, teleost ventricular myocytes also have been purported to have a less developed SR than that seen in mammalian cardiomyocytes. In contrast, teleost atrial myocytes have an extensive SR but still lack T-tubules (Santer 1974, Vornanen, Shiels et al. 2002).

In adult zebrafish (ZF; *Danio rerio*) ventricular cardiomyocytes, Ca^{2+} influx from the $Ca_V1.2$ is the major contributor to E-C coupling. A 5-fold larger calcium current ($I_{Ca,L}$) density was observed in ZF ventricular myocytes when compared to $I_{Ca,L}$ densities observed in mammalian cardiomyocytes (Hove-Madsen, Prat-Vidal et al. 2006, Ozdemir, Bito et al. 2008, Zhang, Llach et al. 2011). In human cardiomyocytes, both the voltage-dependence of the Ca^{2+} transient amplitude and cell-shortening resemble the bell-shaped curve of $I_{Ca,L}$. The peak densities are achieved around zero mV in mammalian cardiomyocytes which suggests that $I_{Ca,L}$ is the major contributor to cell-shortening (Bers 2002). In ZF ventricular myocytes, calcium transients measured and cell shortening showed a monophasic increase and reached a plateau at membrane potentials that were well above 0 mV (Zhang, Llach et al. 2011). The calcium influx mediated by the NCX exchanger of trout atrial myocytes could also initiate cell shortening that increased steadily at more positive membrane potentials even when the $I_{Ca,L}$ was abolished with nifedipine (Hove-Madsen, Llach et al. 2000, Hove-Madsen, Llach et al. 2003).

Thus the source of cytosolic Ca^{2+} for E-C coupling differs between mammalian and teleost species. The increase in cytosolic Ca^{2+} that binds to cTnC and lead to muscle contraction is contributed by the L-type calcium channel (10-40% depending on the species) and from the SR (60-90%) via ryanodine receptors (Bers 2002, Van Petegem 2012). In teleosts, however, the mechanism appears to differ between different

teleost species. As seen in ZF and Crucian carp ventricular cardiomyocytes, the major source of Ca^{2+} for E-C coupling is largely from the L-type calcium channel and less so from the SR (Vornanen 1997, Zhang, Llach et al. 2011).

1.3. Cardiac TnC and skeletal slow-specific TnC in ZF heart

When Sogah *et al.*, knocked out either or both *tnnc1a* (cTnC) and *tnnc1b* (ssTnC) it resulted in abnormalities in heart contraction and chamber morphology (Sogah, Serluca et al. 2010). The group chose the recessive lethal mutations *sil*^{m656} and *sil*^{sk25} from a large-scale zebrafish genetic screen to study the defects in ventricular contractility observed in zebrafish (Stainier, Fouquet et al. 1996). The mutant ZF displayed a larger atrium compared to wild-type while the ventricle exhibited a more compact and distorted shape. Myofibrils also failed to form properly in ventricular tissues. As ZF embryo development progressed, the ventricle also ceased to contract (Stainier, Fouquet et al. 1996, Sogah, Serluca et al. 2010).

The authors used linkage and positional cloning studies to identify that the gene, *tnnc1a*, was involved in cardiac contractility and the morphology defects observed in ZF. While using whole-mount in situ hybridization to detect where *tnnc1a* mRNA transcripts were predominantly expressed, they found another distinct population of transcripts. Relying on the expressed sequenced tags (ESTs) for ZF and further analysis, the authors identified and confirmed the identity of a new paralog, *tnnc1b*. They found that *tnnc1a* was predominantly expressed in the heart and more specifically, in the ventricular chamber. *tnnc1b* was found in slow skeletal muscle. Tol2 transposase mRNA constructs containing wild-type *tnnc1a* were injected into mutant ZF embryos that were heterozygous for *sil*^{m656} or *sil*^{sk25}. The abnormal contractility observed in mutant ventricles was rescued. This further supports the notion that the heart defects were caused by disruption of the *tnnc1a* gene (Sogah, Serluca et al. 2010).

Knock down of *tnnc1a* and *tnnc1b* expression in ZF embryos resulted in abnormal ventricular and atrial contractility, respectively. Morphilinos, short oligonucleotides used as in anti-sense knockdown technique, were employed to reduce *tnnc1a* or *tnnc1b* expression (Bill, Petzold et al. 2009). Surprisingly, atrial contraction

was still observed when expression of *tnnc1a* was suppressed even though ventricular contraction and morphology were severely affected. Injection of a *tnnc1b* morpholino did not affect ventricular contraction but no blood circulation was observed. Reducing both *tnnc1a* and *tnnc1b* expression completely inhibited contraction of both chambers. Results from these studies imply that *tnnc1b* is not only expressed in slow skeletal muscle but is also expressed in the atrium of embryonic ZF. *tnnc1b* expression also plays an important role in atrial contraction and subsequently, blood circulation (Sogah, Serluca et al. 2010).

Genge *et al.* did a further study into *tnnc1a* and *tnnc1b* mRNA expression levels in the adult ZF atrium and ventricle chambers at various acclimating temperatures. qPCR methods were used to measure the mRNA expression levels in each heart chamber in fish adapted for at least two weeks at either 18°C or 28°C. The $\Delta\Delta C_t$ method was used and the geometric mean of two housekeeping genes, β-actin and elongation factor-1 alpha, were used to normalize the data. At 18°C, the expression level for *tnnc1a* was much higher than *tnnc1b* higher in both the atrium (1.5-fold higher) and the ventricle (300-fold higher). However at 28°C, *tnnc1b* expression was 2-fold higher in the atrium than *tnnc1a*. The expression level for *tnnc1a* was still higher than *tnnc1b* in the ventricle at 28°C but by 150-fold higher, rather than 300-fold (Genge, Davidson et al. 2013).

Teleosts have three TnC genes: *tnnc1a*, *tnnc1b* and *tnnc2* that encode for cTnC, ssTnC and fsTnC, respectively. In mammalian species, there are only two genes for TnC: *tnnc1* and *tnnc2* that encode for cTnC and fast-skeletal TnC (fsTnC), respectively (Gordon, Homsher et al. 2000). Through a series of phylogentic analysis, Genge *et al.* was able to identify and confirm that *tnnc1b* is found in all teleost genomes sequenced to date and is distinct from *tnnc1a* (Genge, Davidson et al. 2013). Genge *et al.* proposed that this paralog occurred by tandem gene duplication since both paralogs exist on the same chromosome. The authors also speculated that the differential gene expression observed in the two chambers at the two temperatures may play a role in the teleost adaptive capabilities to the species' living conditions (Genge, Davidson et al. 2013). However, further functional studies would need to be conducted to investigate whether cTnC and ssTnC display different functional properties at different temperatures.

1.4. The troponin complex and cardiac muscle contraction

The cardiac troponin (cTn) complex plays a crucial role in regulating muscle contraction in the heart. cTn is part of a larger component called the thin filament, which is largely made up of polymerized actin and tropomyosin (Figure 1.4.1). cTn is bound and located at approximately every seventh actin molecule on the actin polymer chain. Cardiac troponin C (cTnC), cardiac troponin I (cTnI), and cardiac troponin T (cTnT) make up the cTn complex. cTnC is the Ca^{2+}-binding subunit of the complex. As cytosolic Ca^{2+} increases from approximately 100 nanomolar to high nanomolar or even micromolar concentrations, the regulatory site of cTnC binds to Ca^{2+} and leads to muscle contraction. cTnI is the inhibitory subunit of the complex and binds to actin to inhibit actomyosin ATPase activity during resting or diastolic Ca^{2+} concentrations in the cell. It also plays a structural role of anchoring the cTn complex to the thin filament. cTnT is the tropomyosin binding subunit in the cTn complex. cTnT plays a structural role in bringing cTnC and cTnI together by various interactions and anchors the cTn complex onto the thin filament through its interaction with tropomyosin (Gordon, Homsher et al. 2000).

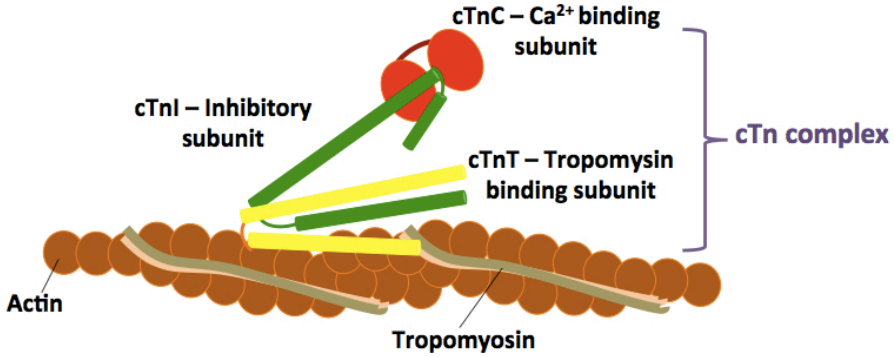

Figure 1.4.1 Cartoon image of the thin filament containing the cardiac troponin complex (cTn: cTnC, cTnI and cTnT), actin polymer and tropomyosin.

The molecule shown in in red is cTnC, in green is cTnI, in yellow is cTnT. The actin polymer is represented by brown-filled circles. Tropomyosin is represented as two strands shown in pink and ash-brown.

Takeda *et al.* solved the structure of the cTn complex in a Ca^{2+}-saturated state using X-Ray crystallography. Each of the cTn subunits is α-helical in structure. cTnC is made up of nine helices. cTnI is made up of three helices and cTnT is made up of two

helices (Figure 1.4.2). The cysteines residues (Cys35/Cys84) were mutated to serines in cTnC, and truncated cTnI and cTnT were used to solve the structure. Electron density for several regions was also insufficient for analysis. This may mean that there are more secondary structural elements in the proteins than are accounted for in the X-Ray structure. The N-terminal domain of cTnI (residues 43-65) interacts with the C-lobe of cTnC. cTnI (residues 66-79) interacts with cTnT. cTnI (90 to 135) also interacts with cTnT in a parallel α-helical coiled-coil fashion. A region called the regulatory domain of the cTn complex includes all three subunits coming together (Figure 1.4.2). The structure shows that the C-terminal domain of cTnC interacts with C-terminal domain of cTnI. This structure corroborates the proposed mechanism by which muscle contraction occurs when Ca^{2+} binds to the regulatory site of cTnC (Takeda, Yamashita et al. 2003).

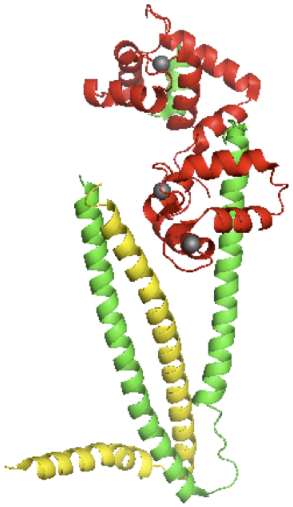

Figure 1.4.2 Cartoon diagram of the human cTn complex
Structure of the core domain of cTn complex in Ca^{2+}-bound form solved by using X-Ray crystallography. Structure in red is cTnC. Structure in green is cTnI. Structure in yellow is cTnT. PDB: 1J1E (Takeda, Yamashita et al. 2003). Figure was generated using PyMol (Delano 2002).

A series of conformational changes occur when Ca^{2+} is bound to the regulatory domain of cTnC. cTnC contains four EF hands. Site I is dysfunctional and does not bind to any metal ions. Site II is deemed the regulatory site and Ca^{2+} must bind to this site in order for muscle contraction to occur (Putkey, Sweeney et al. 1989, Sweeney, Brito et al. 1990). In the unbound state of site II of cTnC, the inhibitory region of cTnI (residues 137 to 148) is bound to actin and inhibits S1-myosin activity (Talbot and Hodges 1981, Rarick, Tu et al. 1997, Tripet, Van Eyk et al. 1997, Takeda, Yamashita et al. 2003). Upon Ca^{2+} binding to site II of cTnC, a hydrophobic patch on the N-terminal domain of cTnC is

exposed for the switch region of cTnI (residues 149 to 159; helix 3) to bind. The interaction between the switch region of cTnI and cTnC maintains cTnC in its open conformation, which in turn releases the inhibitory region of cTnI from actin (Li, Spyracopoulos et al. 1999, Takeda, Yamashita et al. 2003). This then allows the S1-myosin head of the thick filament to bind to actin, resulting in muscle contraction (Tardiff 2011). Sites III and IV are referred to as the structural sites and are continuously occupied by either Ca^{2+} or Mg^{2+} under physiological conditions (Negele, Dotson et al. 1992, Takeda, Yamashita et al. 2003). These are called the structural sites because the bound metal ions in cTnC co-ordinate cTnT (Asp270) and maintains the C-terminal domain of cTnC in a tightly folded state so it can also interact with N terminal of cTnI (residues 36-64) (Takeda, Yamashita et al. 2003).

1.5. The structure of cTnC

cTnC is a highly conserved protein that is made up of 161 residues. cTnC (*tnnc1*) along with fast skeletal TnC (fsTnC; *tnnc2*) are the two paralogs found in all vertebrate species. cTnC is expressed in both cardiac and slow skeletal tissues while fsTnC is only expressed in fast skeletal tissue. fsTnC is made up of 162 residues and has 65% amino acid identity with cTnC.

cTnC is composed of nine helices and is globular in structure. It contains two lobes (C- and N-lobes) with each lobe containing two of each of the four EF hands. The N-lobe contains sites I and II whereas the C-lobe contains sites III and IV (Figure 1.5.1). Unlike fsTnC that also contains four EF hands that can bind to metal ions, cTnC only has three sites that can bind to metal ions (Gordon, Homsher et al. 2000, Takeda, Yamashita et al. 2003). When the regulatory sites I and II of sTnC are bound to Ca^{2+}, the structure adopts an open conformation where the angle between helices NAD and BC widen to expose a hydrophobic surface (PDB: 1SKT; PDB: 1AVS) (Strynadka, Cherney et al. 1997, Tsuda, Miura et al. 1999). The N-terminal domain of cTnC (cNTnC; residues 1 to 89) was solved by NMR in the absence and presence of cTnC (PDB: 1SPY; PDB: 1AP4) (Spyracopoulos, Li et al. 1997). Unlike fsTnC, cNTnC in the Ca^{2+}-bound state did not show an obvious open conformation. The authors speculated that in fsTnC, the extra Ca^{2+} that can bind to site I is enough to pull helices NAD from the BC helices. It was

shown, however, that in the presence of Ca^{2+}, the cTnI peptide (residues 147 to 163) stabilized cNTnC in the open conformation (Sia, Li et al. 1997, Li, Spyracopoulos et al. 1999).

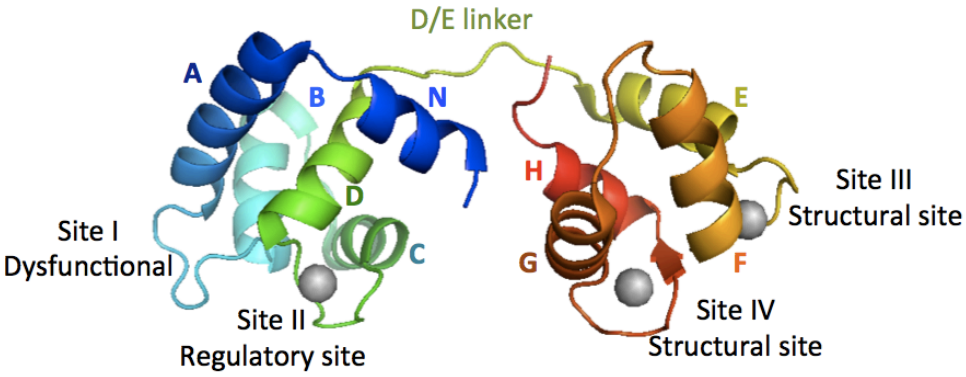

Figure 1.5.1 Cartoon of human cTnC structure
Structure of cTnC solved with Ca^{2+} (grey) bound in sites II, III and IV. 1J1E (Takeda, Yamashita et al. 2003). Figure was generated using PyMol (Delano 2002).

1.6. Previous determination of cTnC Ca^{2+} binding affinity

The binding affinities of cTnC towards Ca^{2+} and Mg^{2+} have been studied using native Tn proteins extracted from bovine heart tissue. Holroyde *et al.* was one of the first groups to determine the molar ratio of cTnC to Ca^{2+} and subsequently, the binding affinities between cTnC and the two metal ions at 4°C. Using equilibrium dialysis, $^{45}CaCl_2$ and scintillation methods, the group was able to determine the binding affinity of each site. They reported that the regulatory site has a Ca^{2+}-specific and low binding affinity of 1×10^5 M^{-1}. The structural sites can bind to either Ca^{2+} with a binding affinity of 1×10^6 M^{-1} or to Mg^{2+} with a binding affinity of 7×10^2 M^{-1}. In the presence of Mg^{2+}, the structural sites have a binding affinity of 3×10^3 M^{-1} towards Ca^{2+}. It is also important to note that when the complex, cTnC-cTnI, was used to determine the binding affinities for all three sites, an increase of binding affinity by ten-fold was seen in each case. In site II, the binding affinity increased to 2×10^6 M^{-1}. In sites III and IV, the binding affinity was increased to 3×10^8 M^{-1}. This suggests that the binding affinities of cTnC for Ca^{2+} and Mg^{2+} are different depending on the interaction of TnC with other components of the thin filament such as TnI, TnT and tropomyosin (Holroyde, Robertson et al. 1980).

1.7. Fluorescence labels/reporters used to determine the binding affinity between cTnC and Ca^{2+}

Another method for determining the binding properties between TnC and Ca^{2+} has been covalent attachment of a fluorescence label to the protein. The protein sample with the attached fluorophore would be excited at the appropriate wavelength followed by Ca^{2+} titration and fluorescence measurement. To determine the increase or decrease in Ca^{2+} sensitivity, the $K_{1/2}$ value, or the [Ca^{2+}] required to elicit half-maximal fluorescence, would be calculated and the pCa_{50} at this point would be compared with other pCa_{50} values from wild-type measurements. Studies have also used fluorescence label attachment to proteins to determine the Ca^{2+} binding affinity (K_a) or the dissociation constant (K_d: where $K_d = 1/K_a$) by measuring the rate of formation and dissociation from steady-state and stopped-flow measurements. The labels used for these studies may include 2-4(4'-(iodoacetamido)aniline)-naphthalene-6-sulfonic acid (IAANS), 5-((2-[iodoacetyl)amino]ethyl)amino)naphalene-1-sulfonic acid (IAEDANS), or N-(2-(iodoacteoxy)ethyl)-N-methyl-amino-7-mitrobenz-2-oxa-1,3-diazole) (IANBD) to measure the binding properties of TnC to Ca^{2+} (Putkey, Liu et al. 1997, Tikunova and Davis 2004, Dong, Xing et al. 2008, Pinto, Parvatiyar et al. 2009). For structures of each label used, please see Figure 1.7.1.

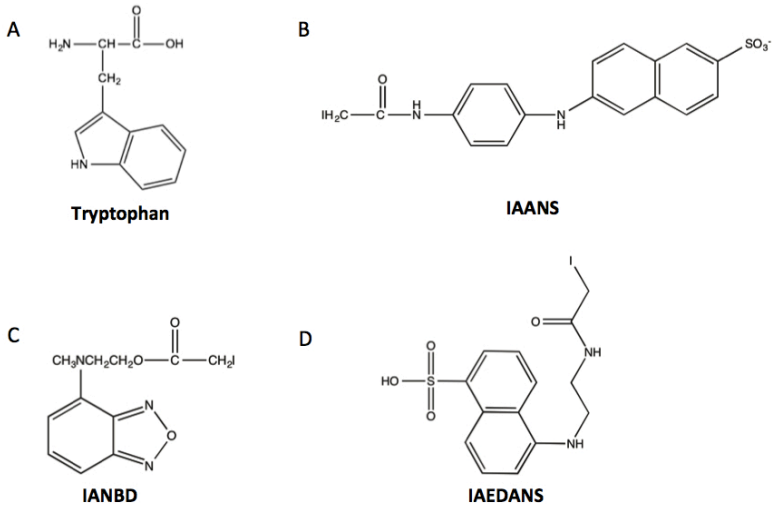

Figure 1.7.1 Structures of tryptophan and other fluorescence labels used to determine Ca^{2+} sensitivity or binding affinity to site II of cTnC
Structures were created using ChemBioDraw (version 13.02.3020; PerkinElmer)

Many Ca^{2+} binding properties of cTnC mutations associated with heart disease such as hypertrophic cardiomyopathy (HCM), restrictive cardiomyopathy (RCM) and dilated cardiomyopathy (DCM) have been studied using these fluorescence labels. HCM is characterized by asymmetrical hypertrophy, myocardial disarray, contractile dysfunction and arrhythmias. The severity of the disease is variable with some individuals remaining largely asymptomatic, while others exhibit severe diastolic dysfunction, heart failure and premature death (Frey, Luedde et al. 2012). The morphology of the heart in an individual with RCM is often normal in appearance, although cases of dilated atria have been observed due to the characteristics of this disease. RCM is characterized by restricted or impaired ventricular filling with abnormal diastolic filling and often normal or close-to-normal systolic function. The disease results in abnormal increase in stiffness of the myocardium leading to sudden rise in pressure within the ventricles with a small increase in volume (Ammash, Seward et al. 2000, Schutte and Essop 2001, Willott, Gomes et al. 2010). DCM is characterized by dilation and contractile dysfunction of the left or both ventricles. This disease may lead to heart failure and only 50% of individuals live beyond five years once diagnosed with DCM (Willott, Gomes et al. 2010).

It was suggested in a review by Willot *et al.* that a trend for Ca^{2+} sensitivity exists for mutations in cTn subunits associated with HCM, RCM and DCM. cTn subunits

associated with HCM and RCM in the isolated form, or in complex with the other cTn subunits, or reconstituted with cTn subunits in skinned fibres tend to display an increase in Ca^{2+} sensitivity whereas DCM tend to display a decrease in Ca^{2+} sensitivity. The increase or decrease in Ca^{2+} sensitivity observed as a result from the diseased cTn subunit have shown to affect its interactions with other subunits and/or thick filament interactions between myosin and actin. It has been implied that the mutations found in cTn subunits and are involved in these cardiomyopathies may predict the whether the subunit may have an increase or decrease in Ca^{2+} or not (Parvatiyar, Pinto et al. 2010, Willott, Gomes et al. 2010). The following sections in this chapter will describe briefly of the Ca^{2+} properties observed using fluorescence labels in previous teleost cTnC studies and studies in cTnC mutations associated with the various cardiomyopathies.

1.7.1. Using tryptophan as a fluorescence reporter for cTnC and Ca^{2+} sensitivity and binding affinity

Measuring the fluorescence emitted by a tryptophan residue in cTnC has been used to compare the Ca^{2+} sensitivity of site II in trout and mammalian cTnC. Due to the fact that cTnC does not contain a tryptophan residue in its sequence, the phenylalanine residue at position 27 has been substituted with a tryptophan in cTnC (F27W cTnC) for these studies. Tryptophan is an aromatic molecule that can be excited at 276 nm and its emission wavelength can be measured at 330 nm (Moyes, Borgford et al. 1996, Gillis, Moyes et al. 2003). Gillis *et al.* was the first group to study teleost cTnC using this method. The authors measured and compared the pCa_{50} values between bovine cTnC (BcTnC) and rainbow trout cTnC. Trout cTnC has thirteen residue differences from its mammalian equivalent and are able to live in temperatures ranging from 2 to 21°C. The purpose of their study was to determine whether the differences in residues seen between these two species contributed to different Ca^{2+} sensitivities of site II of cTnC. The data showed a 2.29-fold increase in Ca^{2+} sensitivity for trout cTnC at 21°C and a decrease in Ca^{2+} sensitivity for both bovine and trout cTnC as temperature decreased from 37°C to 21°C to 7°C at constant pH. The Ca^{2+} sensitivity also increased with increasing pH at a constant temperature of 21°C (Gillis, Marshall et al. 2000). Five residues – asparagine at position 2, isoleucine at position 28, glutamine at position 29, and aspartic acid at position 30 – located in the N-terminal region of trout cTnC may

have influenced this increase in Ca^{2+} sensitivity. Gillis *et al.* further investigated the Ca^{2+} binding properties of trout cTnC with mammalian residues Leu29 and Gly30 using the F27W reporter. Ca^{2+} sensitivity reportedly decreased in the mutant Q29L/D30G trout cTnC compared to that of its mammalian equivalent (Gillis, Moyes et al. 2003).

A further study was done by Liang *et al.* to determine the $K_{1/2}$ values of isolated BcTnC, L29Q BcTnC and the NIQD mutant BcTnC construct. This NIQD mutant contains mutations of residues Asp2, Val28, Leu29, Gly30 to Asn (N), Ile (I), Gln (Q), and Asp (D), respectively. Each of these proteins used the F27W mutation in each cTnC as a reporter to determine these values. Liang *et al.* carried out steady-state and stopped-flow fluorescence measurements. In addition to pCa_{50} values, association rate constants (K_{on}), dissociation rate constants (K_{off}) and dissociation constants (K_d) were also determined. The $K_{1/2}$ of L29Q BcTnC (3.0 ± 0.5 μM) and NIQD BcTnC (2.1 ± 0.3 μM) mutants showed an increase in Ca^{2+} sensitivity by 1.4- and 1.9- fold respectively in comparison to WT BcTnC (4.1± 0.5 μM). The K_d values determined from L29Q BcTnC (8.0 ±1.2 μM) and NIQD BcTnC (5.7 ± 0.6 μM) also supported an increase affinity for Ca^{2+} in comparison to WT BcTnC (11.3 ± 1.3 μM) (Liang, Chung et al. 2008).

Parvatiyar *et al.* also used the F27W cTnC as a reporter to determine the pCa_{50} values of mutant cTnC-associated cardiomyopathies. A23S cTnC is associated with hypertrophic cardiomyopathy (HCM). S37G, V44Q and L48Q mutations in cTnC are associated with restrictive cardiomyopathy (RCM). A23S, V44Q and L48Q all showed increase in pCa_{50} values of 5.98 ± 0.08, 6.29 ± 0.07, and 6.13 ± 0.05, respectively. The mutants showed an increase in Ca^{2+} sensitivity when compared to the wild-type cTnC pCa_{50} value of 5.48 ± 0.02. E40Q and I61Q are associated with dilated cardiomyopathy (DCM). Only the E40A mutant showed a decrease in pCa_{50} value of 5.16 ±0.08, implying a decrease in Ca^{2+} sensitivity. S37G and I61Q had pCa_{50} values of 5.47 ± 0.02 and 5.42 ±0.07, respectively; these mutants did not show a change in Ca^{2+} affinity, indicating that these may have other effects at a higher level of organization (Parvatiyar, Pinto et al. 2010).

1.7.2. Using IAANS as a fluorescence reporter for Ca^{2+} binding affinity of cTnC

Several studies on cTnC have also used IAANS as a fluorophore to measure the fluorescence emitted upon Ca^{2+} titration. IAANS reacts with thiol groups. Its peak excitation wavelength is at 330 nm and its emission wavelength can be monitored at 450 nm. Dweck *et al.* covalently attached IAANS to human Cys84 of cTnC (C84 $cTnC_{IA}$) to measure the Ca^{2+} affinity at the regulatory site of cTnC. The constructs also included the mutation, Cys35Ser, to avoid IAANS attachment to this site and the disease-associated mutations L29Q or G159D (Dweck, Hus et al. 2008). L29Q cTnC is a mutation found in a patient that has familial hypertrophic cardiomyopathy (FHC) (Hoffmann, Schmidt-Traub et al. 2001). G159D cTnC is a mutation found in a patient with dilated cardiomyopathy (DCM). Only minimal changes in pCa_{50} values were observed between WT Cys84 $cTnC_{IA}$ and G159D/Cys84 $cTnC_{IA}$ in the presence and absence of Mg^{2+}. However, a 0.12 increase in pCa_{50} was observed in L29Q/Cys84 $cTnC_{IA}$ (pCa_{50}: 5.30) when compared with WT Cys84 $cTnC_{IA}$ (pCa_{50}: 5.18) in the presence of Mg^{2+}. This implies that L29Q/Cys84 $cTnC_{IA}$ has a higher sensitivity for Ca^{2+}. Upon addition of Ca^{2+}, the fluorescence curve for L29Q/Cys84 $cTnC_{IA}$ also carried a biphasic property unlike the fluorescence curves seen for WT and G159D cTnC in the presence and absence of Mg^{2+}. This suggests that the L29Q/Cys84 $cTnC_{IA}$ construct is binding to two classes of sites and may have structural effects that differ from the other mutant proteins (Dweck, Hus et al. 2008).

Parvatiyar *et al.* used a double IAANS label at positions Cys35 and Cys84 to determine the pCa_{50} values of the A31S cTnC mutations which are associated with HCM. Unlike other HCM mutants, the pCa_{50} value of A31S (4.95 ± 0.01) was lower when compared to the pCa value of wild-type cTnC (5.12 ±0.04). This indicates a decrease in Ca^{2+} sensitivity (Parvatiyar, Landstrom et al. 2012).

Davis *et al.* proposed another IAANS attachment at position 53 by mutating the threonine into a cysteine to determine the binding affinity of Ca^{2+} in site II of cTnC and ssTnC. The two cysteines at positions 35 and 84 were mutated to serines to prevent attachment of IAANS at these positions. Position 53 was chosen for its location in the molecule as Thr53 of cTnC does not directly interact with cTnI, nor does it interact with

the regulatory Ca^{2+}. Fluorescence and stopped-flow measurements were limited to the cTn complex and not on the apo form of cTnC. The K_d values found were 649 nm and 248 nm in cTn and in fast skeletal Tn complexes, respectively (Davis, Norman et al. 2007).

1.7.3. Using IAEDANS and IANBD as a fluorescence reporters for Ca^{2+} binding affinity of cTnC

Dong *et al.* used IAEDANS as a fluorophore to measure the pCa_{50} values of L29Q and G159D cTnC mutants. IAEDANS reacts with thiol groups and has maximal excitation and emission wavelengths of 336 nm and 490 nm, respectively. The group conducted Förster resonance energy transfer (FRET) to monitor Ca^{2+}-induced opening and closing of the N-domain of cTnC on each of the cTnC mutants. The group reconstituted the cTn complex with the cTnC mutants. All tryptophans were removed in from cTnI and none exist in cTnT. Two mutations were introduced into cTnC where L12W was used as the FRET donor and the IAEDANS attached at N51C was used as the FRET acceptor. The pCa_{50} values determined for wild-type, L29Q and G159D cTnC were 5.55 ± 0.06, 5.45 ± 0.04 and 5.65 ± 0.06, respectively. The authors did not see a large effect on pCa_{50} values upon Ca^{2+} titration for both L29Q and G159D mutations. Unlike previous studies, L29Q cTnC in fact displayed a slight decrease in Ca^{2+} sensitivity (see section 1.5.3) (Dong, Xing et al. 2008).

Wang *et al.* saw an increase in Ca^{2+} affinity for the L29Q cTnC mutant. This group used the IANBD fluorophore, which has peak excitation and emission wavelengths of 490 nm and 530 nm, respectively. Cys35Ser mutation was introduced to L29Q cTnC for site-specific labeling of the IANBD fluorophore at Cys84 residue. The pCa_{50} values determined for wild-type and L48Q cTnC were 6.99 ±0.03 and 7.31 ± 0.03, respectively (Wang, Robertson et al. 2012).

1.8. Using CD spectroscopy to observe structural changes in teleost and mammalian cTnC

Circular dichroism (CD) spectroscopy has been used to observe changes in the structural properties of TnC and their T_m. CD spectroscopy measures the differential

absorption of left- and right-handed circularized polarized light from components with chirality that are intrinsic to their structures. A protein consists of α-helices, anti-parallel β-sheets, type I β-turns, random coils or a combination of two or more of these structural elements. Each of the secondary structures has chirality around their peptide bonds and therefore can also absorb left- and right-handed circularized polarized light in the far UV region (240 nm to 180 nm). The spectra given by CD spectroscopy of a particular protein will display characteristics that are related to the secondary structure content of that protein. A protein such as TnC, which has a high α-helical content, will produce a CD spectrum with two absorbance minima at 208 nm and 222 nm (Kelly and Price 2000, Kelly, Jess et al. 2005).

1.8.1. Determining the α-helical content of rainbow trout and Atlantic salmon cTnC using CD spectroscopy

CD spectroscopy was used to observe cTnC structural changes in rainbow trout (*Oncorhynchus mykiss)* and Atlantic salmon (*Salmo salar*) in comparison to mammalian cTnC. The spectra were collected in the presence and absence of Ca^{2+}. In all cases, larger negative shifts were observed at 222 nm in the presence of Ca^{2+}. This indicates that there was an increase in α-helical content. However, it was observed that bovine cTnC had a slightly lower molar ellipticity change, or overall shift in the negative direction, of 3.1 deg $cm^2/dmol^{-1}$ in comparison to trout of 5.5 deg $cm^2/dmol^{-1}$ and Atlantic salmon of 4.4 deg $cm^2/dmol^{-1}$. The mammalian cTnC had a higher α-helical content in the absence of Ca^{2+}. However, the shift in ellipticity was also smaller than that of teleost cTnC. This suggests that mammalian cTnC may be more stable than teleost cTnC because of the higher α-helical content observed in a Ca^{2+}-free environment but teleost cTnC may become more stable in the presence of Ca^{2+} due to the increase in α-helical content observed (Moyes, Borgford et al. 1996). This provides the basis for the direct measurement of teleost and mammalian cTnC melting temperatures in the presence and absence of Ca^{2+} discussed in Chapter 3.

1.8.2. Determining the melting temperature of bovine cTnC using CD spectroscopy

McDubbin *et al*. used CD spectroscopy to determine the T_m of bovine cTnC in three different environments: 1) an environment that was nominally Ca^{2+} free; 2) an environment containing only enough free Ca^{2+} (0.3 μM) that would saturate only the high-affinity sites III and IV of cTnC; and 3) an environment containing enough Ca^{2+} (2 mM) to saturate all three sites on cTnC. In the Ca^{2+}-free environment, cTnC had a T_m of 69°C. In the environment containing only enough Ca^{2+} to saturate the high affinity sites, cTnC had a T_m of 63.5°C. The Ca^{2+}-saturated cTnC had a T_m of 69.5°C. Their data imply that the apo-cTnC is much more stable than the cTnC with sites III and IV occupied. Yet when cTnC had all three sites bound by Ca^{2+}, the protein stability is returned to that of its apo-form (McCubbin, Hincke et al. 1980).

Other studies have shown, using CD spectroscopy, in both mammalian skeletal TnC (sTnC) and cTnC that Ca^{2+} binding to each of the three sites led to an increase in α-helical content (Leavis and Kraft 1978, Leavis, Rosenfeld et al. 1978, Gusev and Barskaya 1984). CD spectroscopy studies on mammalian sTnC and cTnC peptides demonstrate that it is the C-terminal domain of both TnC molecules that contribute most to the increase in α-helical content. Peptides containing only the high-affinity C-termini sites of sTnC and cTnC increase the α-helical content in a solution containing Ca^{2+} or Mg^{2+} (Leavis and Kraft 1978, Leavis, Rosenfeld et al. 1978, Gusev and Barskaya 1984). The N-terminal peptides of both these TnC molecules, however, showed no major shifts in α-helical content. Gusev *et al.* speculated that certain residues flanking the binding sites are not involved in the formation of α-helices until binding of Ca^{2+} or Mg^{2+} occurs (Gusev and Barskaya 1984).

The data gathered from these papers suggest that the Ca^{2+} binding to the two high affinity sites in the C-terminal domain are the source of the majority of the newly formed α-helical content. This further implies that the increase in α-helical content would contribute to a more compact, globular and stable protein. This would also imply that a higher T_m would have been expected for a fully saturated TnC, or with Ca^{2+} present only in the two high affinity sites.

1.8.3. Using CD spectroscopy to observe changes in α-helical content in cTnC mutants that were found to be associated with various cardiomyopathies

Many studies also used CD spectroscopy to observe structural changes in single genetic mutations that have given rise to a variety of cardiac diseases such as HCM, DCM and RCM in comparison to wild-type human cTnC. Changes in α-helical content of each mutant determined by CD spectroscopy were done in an apo condition, Mg^{2+}-bound condition or a Ca^{2+}/Mg^{2+} saturated condition.

Several HCM-associated cTnC mutants including A8V, C84Y, E134D, D145E, A31S and A23Q were studied (Pinto, Parvatiyar et al. 2009, Parvatiyar, Pinto et al. 2010, Parvatiyar, Landstrom et al. 2012). Increases in α-helical content in all three conditions were observed for the A8V mutation. This implies that this residue is involved in stabilizing the helix in the N-terminus of the protein. Also under Ca^{2+} binding fluorescence studies, the A8V mutant showed no increase in fluorescence by itself until addition of tropomyosin and actin. Therefore, Pinto *et al.* speculated that the A8V mutant causes Ca^{2+} binding affects through protein-protein interactions with other proteins of the thin filament of which may have contributed by the stabilized N-terminal helix by A8V (Pinto, Parvatiyar et al. 2009).

There were some cTnC HCM-causing mutants such as A31S and E134D that did not show any change in α-helical content (Pinto, Parvatiyar et al. 2009, Parvatiyar, Landstrom et al. 2012). The A31S cTnC molecule did show an increase in binding affinity for Ca^{2+} in isolated cTnC but the affinity for Ca^{2+} reverted back to that of wild-type cTnC upon addition Tn subunits (Parvatiyar, Landstrom et al. 2012). The authors speculated that E134D mutation in TnC interferes with the phosphorylation of cTnI by protein kinase C because the mutation is in close proximity to the phosphorylation site on cTnI. This may alter the phosphorylation signal and thereby affect the Ca^{2+} binding affinity of cTnC (Pinto, Parvatiyar et al. 2009).

Results from CD spectroscopy of C84Y and D145E mutants showed a decrease in α-helical content under apo conditions. C84Y was stabilized back to wild-type values under Mg^{2+}-bound only or Ca^{2+}/Mg^{2+} conditions. D145E still showed a decrease in α-helical content under Ca^{2+}/Mg^{2+}-saturated conditions. The authors speculated that these

residues decrease the stability of cTnC and therefore, have an effect on Ca^{2+} binding. They further speculated that the mutations interfere with the normal interactions with cTnI due to the positioning other mutants with relation to cTnI (Pinto, Parvatiyar et al. 2009).

CD spectroscopy was also used to study the change in α-helical content in RCM- and DCM-associated mutations in cTnC. S37G, V44Q and L48Q cTnC are RCM-associated mutations. Only V44Q showed an increase in α-helical content under apo and Ca^{2+}/Mg^{2+} conditions while S37G and L48Q cTnC mutants showed no structural changes. These mutations may have an effect at a higher-level of organization as in they may alter or interfere with other interactions with the subunit or thin filament, thereby effecting thin filament regulation. E40Q and I61Q cTnC mutants are DCM-associated mutations. Both cTnC mutants showed a decrease in α-helical content. The structural changes observed for RCM- and DCM-associated cTnC mutants may explain the increase and decrease, respectively, of Ca^{2+} affinity observed with relation to the structural changes observed (Parvatiyar, Pinto et al. 2010).

1.9. Experimental Approaches

The objective of this study is to develop a better functional understanding of why the temperature- and chamber-specific expression of ZF cTnC and ssTnC were observed in previous studies. Genge et al.'s study observed differential and chamber-specific expressions of ZF cTnC and ssTnC at varying temperatures. In the ZF atrium, particularly, it was shown that there was a two-fold increase in ssTnC when temperature of 18°C was raised to 28°C (Genge, Davidson et al. 2013). Thus far, there is no functional explanation as to why an increase in ssTnC was seen with increasing temperature. The eighteen residue differences between the two paralogs may contribute to different Ca^{2+} binding affinities (Figure 1.9.1). Determining the Ca^{2+} binding affinities at site II for each paralog will likely provide a better understanding of the teleological reasons for the differential temperature- and chamber-specific expression patterns observed in ZF.

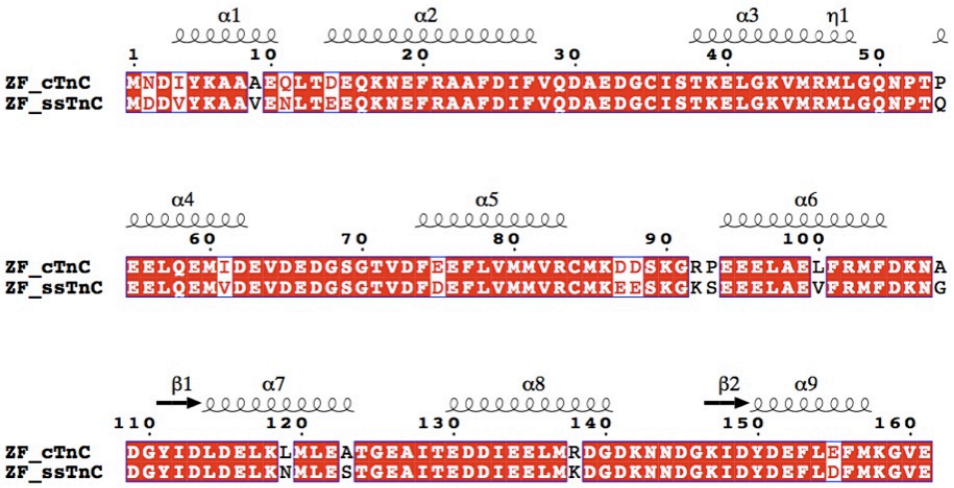

Figure 1.9.1 Sequence alignment of ZF cTnC and ssTnC
Sequence alignment of ZF cTnC (UniProt ID: Q800V7) and ssTnC (UniProt ID: Q6IQ64). Red boxes show absolutely conserved residues and red text shows conservative substitutions. The secondary structures are shown above the sequence. The figure was generated by using ESPript 3.0 (Gouet, Robert et al. 2003) with an alignment file created from Clustal Omega (Sievers, Wilm et al. 2011).

The N-terminal domains consisting of residues 1 to 89 of ZF cTnC (cNTnC) and ssTnC (ssNTnC) were cloned, expressed and purified. The N-terminal domains of ZF TnC contain only sites I and II so that the Ca^{2+} binding properties of site II in ZF cTnC and ssTnC can be determined. Whether site I of ZF ssTnC binds to Ca^{2+} is also unknown, thus this N-terminal domain will also help elucidate whether Ca^{2+} can bind to site I of ZF ssTnC. Isothermal titration calorimetry (ITC) was used to measure the thermodynamic properties for each ZF NTnC construct. In addition to the binding affinity (K_a), the change in entropy (ΔS), change in enthalpy (ΔH), Gibb's energy (ΔG) and the stoichiometry value (*n*) can be computed. For a background description of ITC, see section 2.6.1. For details of protocol, please see section 2.6.

A thermofluor assay was used to determine the stability of full-length cTnC and ssTnC. Sypro-orange was used as a fluorescent dye to monitor the unfolding of each protein with respect to temperature. The T_m, or the midpoint of temperature of protein unfolding, was determined by taking the maxima from the first derivatives of the melting curves.

1.9.1. Background to isothermal titration calorimetry (ITC)

ITC is a method used to directly measure the interaction between two molecular components. Fluorescence labels that may jeopardize the structural and functional integrity of the molecule are not required for the study. The binding affinity of an interaction can be directly measured based on the heat absorbed or released from the reaction. The stoichiometry (N), binding affinity (K_a), enthalpy (ΔH), entropy (ΔS), and Gibb's free energy (ΔG) can be obtained from a single ITC experiment (Leavitt and Freire 2001).

The components that are being studied are in solution. The addition of the first component (i.e. ligand) is injected into the sample cell containing the second component (i.e. protein). Heat signals observed during this process reflect the occurrence of an interaction of the two components (Leavitt and Freire 2001).

The instrument is based on a power compensation principle. The sample cell is held at constant temperature. When an interaction occurs upon injection of the ligand into the protein sample, heat is released or absorbed. The instrument detects the heat change in the sample cell and applies power (μcal/second) to the control heater to keep the sample cell at constant temperature (Freyer and Lewis 2008).

The heat that is released when a reaction occurs during an injection is proportional to the amount of ligand that binds to the protein. At subsequent injections of ligand, the raw heat signals shown as peaks become smaller and smaller as the protein in the sample cell becomes saturated with the ligand. The raw heat signals are integrated to obtain the heat (Leavitt and Freire 2001).

The thermodynamic parameters are based on established reactions at equilibrium and thermodynamic relationships:

$$A + B \rightleftharpoons AB$$

$$K_a = \frac{[AB]}{[A][B]}$$

$$\Delta G = \Delta H - T\Delta S$$

$$\Delta G^o = RT \ln K_{eq}$$

where ΔG^o is the free energy of A in the standard state.

The raw data from an ITC experiment are analyzed using Origin (OriginLab) software. The equations mentioned above and their derivatives are implemented in the software. The raw data are integrated and fitting of the curve is done automatically (Wiseman, Williston et al. 1989, Freyer and Lewis 2008).

1.9.2. Background to Sypro orange

Sypro Orange (Invitrogen) was used as the fluorescence dye to determine the unfolding transition of each protein in terms of absorbance with respect to temperature. Sypro Orange has a maximal excitation and emission wavelengths of 490 nm and 575 nm, respectively. When the fluorescence dye is in an aqueous solution, the fluorescence is quenched. As the hydrophobic core of a protein becomes more exposed, the fluorophore increases its fluorescence emission as the protein continues to unfold. Small volumes (30 to 50 μL) of protein are needed for this assay. It is also straightforward and fast to perform (Ericsson, Hallberg et al. 2006, Nettleship, Brown et al. 2008)

1.10. Aims

Our aims include:

1. Determining the Ca^{2+} binding affinity of site II of ZF cTnC at 28°C, 18°C and 8°C using ITC.
2. Determining the Ca^{2+} binding affinity of site II of ZF ssTnC at 28°C, 18°C and 8°C using ITC.
3. Determine the T_m of each ZF TnC paralog using a thermofluor assay.

1.11. Hypotheses

We hypothesize that:

1. ZF ssTnC has one regulatory binding regulatory site.

2. Each ZF NTnC paralog will have an increase in Ca^{2+} binding affinity with increasing temperature.
3. The ZF NTnC paralog expressed to the greatest degree at lower temperatures (ZF cTnC) will have a higher Ca^{2+} binding affinity.
4. The ZF TnC paralog expressed at an overall higher level (ZF cTnC) will have a higher T_m.

Chapter 2. Materials and Methods

2.1. Mutagenesis of full-length zebrafish TnC constructs

Full-length zebrafish (ZF) cardiac troponin C (cTnC; *tnnc1a*) and full-length ZF slow skeletal troponin C (ssTnC; *tnnc1b*) were synthesized by geneART (Life Technologies) with the F27W reporter and cloned into pET-21a(+) vectors (Novagen). Site-directed mutagenesis (SDM) was used to revert the F27W mutations in both TnC proteins back to wild-type (ZF cTnC and ssTnC: W27F) and transformed into DH5α cells. See Table 2.1.1 for a list of the primers that were used. SDM was performed using instructions from the Phusion Site-Directed Mutagenesis manual (Thermo Scientific). Each construct was sequenced after SDM to verify that the inserted genes were correct.

Table 2.1.1 ZF cTnC and ssTnC forward and reverse primer sequences used to perform site-directed mutagenesis

Construct mutations	Primer sequence
ZFcTnC_W27F_F	5'-gcagcctttgatatttttgttcaggatgcag-3'
ZFcTnC_W27F_R	5'-acgaaattcatttttctgttcatcggtcagctg-3'
ZFssTnC_W27F_F	5'-cagcctttgatatttttgttcaggatgcag-3'
ZFssTnC_W27F_R	5'-cacgaaattcatttttctgttcttcggtcag-3'

*F refers to forward primer. R refers to reverse primer

2.2. Cloning the N-domains of zebrafish cTnC and ssTnC

The constructs containing the N-terminal domains of TnC, comprised of residues 1 to 89, for each of ZF cTnC and ssTnC (cNTnC and ssNTnC) were made using the

ligation-independent cloning (LIC) method (Aslanidis and de Jong 1990). The ZF NTnC genes were cloned into a vector containing a hexahistidine tag, maltose-binding protein and tobacco etch virus (TEV) protease cleavage site upstream of the gene insertion site. Please refer to Table 2.2.1 for the list of primer sequences used in this procedure. Plasmids containing our inserts of interest were transformed into DH5α cells. Plasmids were sequenced to confirm presence of ZF cNTnC and ssNTnC genes (Figure 2.2.1). Vectors, reagents and LIC protocol were kindly provided by Dr. Van Petegem's lab from the University of British Columbia.

Table 2.2.1 ZF NTnC primer sequences

Construct	Primer sequence
ZFcNTnC_F*	5'-tacttccaatccaatgcaaatgatatttataaagcc-3'
ZFcNTnC_R*	5'- ttatccacttccaatgttattagctatcatctttcatgcagcg-3'
ZFssNTnC_F*	5'-tacttccaatccaatgcagatgatgtttataaagcagcc-3'
ZFssNTnC_R*	5'-ttatccacttccaatgttattaagattcttctttcatgcagcg-3

*F refers to forward primer. R refers to reverse primer

A **6-His-MBP-ZF cNTnC**

MGSSHHHHHHGSSMKIEEGKLVIWINGDKGYNGLAEVGKKFEKDTGIKVTVEHPDKLEEKFPQV
AATGDGPDIIFWAHDRFGGYAQSGLLAEITPDKAFQDKLYPFTWDAVRYNGKLIAYPIAVEALSLI
YNKDLLPNPPKTWEEIPALDKELKAKGKSALMFNLQEPYFTWPLIAADGGYAFKYENGKYDIKDV
GVDNAGAKAGLTFLVDLIKNKHMNADTDYSIAEAAFNKGETAMTINGPWAWSNIDTSKVNYGV
TVLPTFKGQPSKPFVGVLSAGINAASPNKELAKEFLENYLLTDEGLEAVNKDKPLGAVALKSYEEEL
AKDPRIAATMENAQKGEIMPNIPQMSAFWYAVRTAVINAASGRQTVDEALKDAQTNSSSNNN
NNNNNNNLGIEENLYFQSNAMNDIYKAAAEQLTDEQKNEFRAAFDIFVQDAEDGCISTKELGK
VMRMLGQNPTPEELQEMIDEVDEDGSGTVDFEEFLVMMVRCMKDDS

B **6-His-MBP-ZF ssNTnC**

MGSSHHHHHHGSSMKIEEGKLVIWINGDKGYNGLAEVGKKFEKDTGIKVTVEHPDKLEEKFPQ
VAATGDGPDIIFWAHDRFGGYAQSGLLAEITPDKAFQDKLYPFTWDAVRYNGKLIAYPIAVEALS
LIYNKDLLPNPPKTWEEIPALDKELKAKGKSALMFNLQEPYFTWPLIAADGGYAFKYENGKYDIK
DVGVDNAGAKAGLTFLVDLIKNKHMNADTDYSIAEAAFNKGETAMTINGPWAWSNIDTSKVN
YGVTVLPTFKGQPSKPFVGVLSAGINAASPNKELAKEFLENYLLTDEGLEAVNKDKPLGAVALKSY
EEELAKDPRIAATMENAQKGEIMPNIPQMSAFWYAVRTAVINAASGRQTVDEALKDAQTNSSS
NNNNNNNNNNLGIEENLYFQSNAMDDVYKAAVENLTEEQKNEFRAAFDIFVQDAEDGCIST
KELGKVMRMLGQNPTQEELQEMVDEVDEDGSGTVDFDEFLVMMVRCMKEES

C

Figure 2.2.1 Presence of 6-His-MBP-ZF NTnC Fusion Protein Confirmed.
Plasmids containing 6-His-MBP-ZF NTnC were confirmed through sequencing. DNA sequences were analyzed using ExPASy Translate Tool (Artimo, Jonnalagedda et al. 2012). A. Sequence of 6-His-MBP-ZF cNTnC fusion protein. B. Sequence of 6-His-MBP ZF ssNTnC fusion protein. C. Cartoon image of 6-His-MBP-ZF NTnC fusion protein.

2.3. Expression of full-length zebrafish cTnC, ssTnC, cNTnC and ssNTnC

For expression of ZF cTnC, ssTnC, cNTnC and ssNTnC protein, each construct was transformed into BL21 (DE3) cells. Colonies from each transformation were cultured and protein production induced with IPTG to test for expression. Expression levels were visualized by SDS-PAGE. A negative control containing cultures grown in the absence of IPTG was also visualized by SDS-PAGE.

Transformed BL21 (DE3) cells were grown in 100 mL of LB with ampicillin (ZF cTnC/ssTnC: 100 µg/mL final concentration) or kanamycin (ZF cNTnC/ssNTnC: 50 µg/mL final concentration) overnight for approximately 16 hours in a shaker at 37°C with

shaking at 250 rpm. 10 mL of overnight culture were inoculated into 1 L of LB with ampicillin/kanamycin. The culture was incubated for 3 hours at 37°C with shaking at 250 rpm. Protein translation was then induced with isopropyl β-D-1-thiogalactopyranoside (IPTG) to a final concentration of 1 mM. Cells were incubated to grow for a further 3 hours at 37°C with shaking at 250 rpm. Cells were then harvested by centrifugation at 6000 x g for 10 minutes at 4°C. The supernatant was discarded and the pellet was stored at -80°C.

The pellet from one litre of culture was resuspended in 30 mL of cold Resuspension Buffer (in mM: 50 Tris, 2 EDTA, 1 DTT, 1 PMSF and 1 complete protease inhibitor tablet (Roche) and pH 7.5). The cell suspension was placed on ice and lysed by sonication with 4 or 5 pulses at 80% amplitude for 20 seconds per pulse. The cell lysate was then centrifuged at 26,953 x g in a Beckman JA17 rotor for 30 minutes at 4°C. The lysate supernatant was decanted for purification.

2.4. Purification of full-length ZF cTnC and ssTnC

Ammonium sulfate (30 grams/100 mL of supernatant) was added slowly to the supernatant containing ZF cTnC or ssTnC while stirring on ice over 30 minutes. The suspension was then centrifuged at 26,953 x g in a Beckman JA17 rotor for 30 minutes at 4°C. The supernatant was transferred to dialysis tubing (MWCO: 3000 Da; Fisherbrand) and dialyzed twice (at least once overnight) against 4 L of Running Buffer (at least once overnight) in 4 L of Running Buffer (25 mM Tris, pH 8.0, 6 M Urea, 1 mM EDTA and 14 mM BME) at 4°C. The sample was then filtered (0.45 μm syringe filter; Whatman) and warmed to room temperature. The sample was then loaded onto either a DE52 (Sigma-Alderich) or DEAE-Sephracryl (Sigma-Alderich) anion exchange column at room temperature. The protein was eluted with High Salt Running Buffer (25 mM Tris, pH 8.0, 500 mM KCl, 6 M Urea, 1 mM EDTA and 14 mM BME). Fractions containing pure protein of interest were pooled together and transferred into dialysis tubing (MWCO: 10, 000 Da; Fisherbrand) and was dialyzed 5 times (at least overnight three times) against 4 L of deionized water. The sample was then concentrated and dialyzed against 2 L of HEPES Buffer (50 mM HEPES, pH 7.2, 150 mM KCl and 10 mM BME). The ZF ssTnC was subsequently purified by size exclusion chromatography using a

HiPrep 26/60 Sephracryl S-100 (GE Healthcare) column. Purified proteins were stored at -80°C.

2.5. Purification of zebrafish cNTnC and ssNTnC by column chromatography

Supernatant containing either ZF cNTnC or ssNTnC was then applied to a cobalt affinity column (ClonTech: TALON Superflow™ Metal Affinity Resin). A bed volume of 5 mL was of cobalt beads was used and was equilibrated with HEPES buffer (50 mM HEPES, 150 mM KCl, 10 mM BME). The column was washed with 5 column volumes of HEPES buffer. The protein was eluted with 300 mM of imidazole in HEPES buffer. To cleave the hexahistidine-MBP moiety, a 6-his tagged TEV protease was added to the pooled fractions containing the tagged protein transferred to dialysis tubing (MWCO: 3000 Da; Fisherbrand). This was dialyzed against 4 L of HEPES buffer overnight. The dialyzed sample was then applied to an amylose column (New England Biolabs: Amylose Resin; 5 mL bed volume), which have been equilibrated and washed with 5 column volumes of HEPES buffer, to remove 6-his-MBP tag. The flow through containing the protein and TEV protease was then applied to a cobalt column, which had been equilibrated and washed with 5 column volumes of HEPES buffer, to remove the residual 6-his-MBP tag and 6-his tagged TEV-protease. The flow through and wash fractions were further purified by size exclusion chromatography using a HiPrep 26/60 Sephracryl-100 HR column (GE Healthcare). Fractions containing the protein of interest were collected and pooled. Purified proteins were stored at -80°C, or prepared for ITC as described in section 2.5.

2.6. Preparation of ZF NTnCs for isothermal titration calorimetry

2.6.1. Sample preparation for isothermal titration calorimetry

Samples containing either ZF cNTnC or ZF ssNTnC were thawed and supplemented with EDTA to a final concentration of 10 mM. The sample was rocked

gently for 3 hours, concentrated by centrifugation (10 kDa MWCO; Fisherbrand) and dialyzed against 4 L of HEPES buffer (50 mM HEPES, pH 7.2, 150 mM KCl and 10 mM BME) 6 times (at least 2 times overnight) to remove the EDTA. All of the above procedures were performed at 4°C. Each sample was centrifuged at 13,000 rpm on a table-top centrifuge (Eppendorf) at 4°C for 15 minutes. The supernatant was then transferred to a new chilled 1.5 mL Eppendorf tube.

2.6.2. Determination of protein concentration using the Edelhoch method

ZF cNTnC and ssNTnC protein samples were diluted 3- and 5-fold their concentrations with guanidine hydrochloride buffer (6 M guanidine hydrochloride, 20 mM sodium phosphate, pH 6.5). Absorbance for each sample was measured at 280 nm with a UV spectrophotometer. TnC does not contain any tryptophan residues; therefore, the molar extinction co-efficient used for the tyrosine residue, 1280 M^{-1} cm^{-1}, was used to determine the ZF NTnC concentrations (Edelhoch 1967).

2.7. Isothermal titration calorimetry on ZF NTnC constructs

ITC was done on ZF NTnC constructs. All ITC experiments were performed on a MicroCal iTC200 (GE Healthcare) instrument. A final concentration of 200 μM of ZF NTnC was used in the sample cell. 1 μL injections (40 injections in total) of 4 mM Ca^{2+} was titrated into the sample with 120 seconds spacing between each injection and a stirring speed of 1000 rpm. Experiments were also done with 200 μM of ZF NTnC and 2 μL injections (20 injections in total) of 2 mM Ca^{2+} with 120 seconds spacing between injections at 1000 rpm. Experiments were performed at 8°C, 18°C and 28°C. Three protein batches were used for ZF cNTnC ITC experiments while only two protein batches were used for all ZF ssTnC ITC experiments. The ligand background was obtained by titrating micromolar amounts of Ca^{2+} into the buffer. The data from the ligand were averaged and subtracted from the Ca^{2+} into ZF NTnC ITC data. Origin 7.0 (OriginLab) was used to analyze binding isotherms.

2.7.1. Verification of the integrity of ZF cNTnC following ITC using size exclusion chromatography

A sample containing ZF cNTnC and Ca^{2+} following ITC was applied to a size exclusion chromatography using a HiPrep 26/60 Sephracryl-100 HR column (GE Healthcare).

2.8. Protein thermal melts on full-length zebrafish cTnC and ssTnC

Protein samples were loaded into a 96-well plate. Each well contained a total of 30 µL of 0.5 mg of ZF ssTnC or 1 mg of ZF cTnC, 2.5 µL of 100-fold dilution of Sypro Orange dye (Invitrogen, 50 mM HEPES (pH 7.2), 150 mM KCl and 14 mM β-mercaptoethanol. Melting curves were done on an MJ Mini Personal Thermal Cycler – Mini Opticon Real-Time PCR System (BioRad) using the SYBR green filter. The BioRad CFX Manager was used to export data into an Excel spreadsheet. A temperature range from 25°C to 95°C was used with 0.5°C increments. Each temperature was held constant for 15 seconds. Seventeen ZF cTnC reactions and eleven ZF ssTnC reactions were used to determine each protein's T_m.

The melting curves were normalized. The lowest absorbance value (Abs_{min}) was subtracted from each value ($Abs - Abs_{min}$). The maximum (Abs_{max}) was determined from the subtracted values. Each subtracted value was then divided by the maximum subtracted value ($(Abs - Abs_{min})/Abs_{max}$) determined.

Each T_m was determined by taking the maxima of the first derivative of the melting curve. An unpaired Student's t-test was used to determine the *p-value* of the two sets of data to see whether the determined T_m for each protein was significantly different from each other.

Chapter 3. Results

3.1. Determination of Ca^{2+} binding affinity of site II in ZF cNTnC and ssNTnC using isothermal titration calorimetry

The Ca^{2+} binding affinity of the regulatory site of ZF TnC has never been determined before. There are eighteen residues difference between cTnC and ssTnC (Figure 1.9.1). To study the interaction between site II and Ca^{2+}, the N-domain of ZF cTnC (ZF cNTnC) and ssTnC (ZF ssNTnC) were cloned, expressed and purified. The N-domain contains residues 1 to 89 of which there are 10 residues different between ZF cNTnC and ssNTnC. The N-domain of each construct also contains only sites I and II where site II is the regulatory site and excludes sites III and IV. Site I of ZF ssTnC has never been previously investigated for interaction with Ca^{2+}. ITC was also used to determine whether Ca^{2+} can bind to both sites I and II or just site II in ZF ssNTnC.

3.2. Cloning and expression of ZF cNTnC and ssNTnC

The cloning and expression of ZF cNTnC and ssNTnC were successful. The final constructs based on the LIC vector contained a 6-his-MBP, and TEV protease cleavage sequence in addition to wild type ZF cNTnC or ssNTnC as confirmed by DNA sequencing (Figure 2.2.1). Each ZF NTnC fusion protein was determined to be close to its predicted molecular weight of 55 kDa. Expression levels were visualized by SDS-PAGE. Bands were observed at a molecular weight of 55 kDa in lanes containing IPTG-induced cultures (Figure 3.2.1). A negative control containing cultures grown in the absence of IPTG was also visualized by SDS-PAGE. The 55 kDa band was absent in these lanes (Figure 3.2.1).

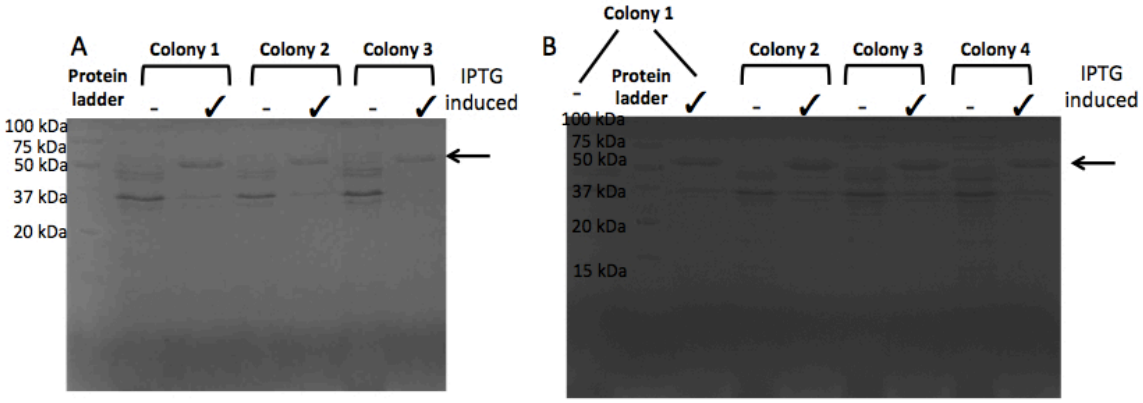

Figure 3.2.1 Expression test for 6-his-MBP-ZF NTnC fusion proteins.
SDS-PAGE visualization of the protein expression test. Bands were observed at 55 kDa. A. Expression of 6-His-MBP ZF cNTnC fustion protein. B. Expression of 6-His-MBP ZF ssNTnC fustion protein. (✓) indicates addition of IPTG. (-) indicates absence of IPTG. Prominent bands in IPTG induced lanes are seen at approximately 55 kDa as indicated by arrow.

3.2.1. Purification of ZF cNTnC and ssNTnC

Proteins were purified as described in section 2.5.1. A prominent band was seen at 55 kDa indicating that the fusion protein bound and eluted successfully from the cobalt column (Figure 3.2.2A: see lane “E-300 mM Imidazole”; Figure 3.2.3A: see lane “E-300 mM Imidazole”). The eluate before and after proteolytic removal of the tag was collected and visualized by SDS-PAGE. Two prominent bands were seen at 45 kDa and 10 kDa indicating the presence of the 6-His-MBP tag and ZF NTnC, respectively, on the SDS-PAGE gel (Figure 3.2.2A: see lane “ZF cNTnC + TEV protease; Figure 3.2.3A: see lane “ZF ssNTnC +TEV protease”). The removal of tag from ZF NTnC protein was confirmed by SDS-PAGE (Figure 3.2.2A: see lane “E-500 mM maltose – Amyl. column”; Figure 3.2.3A: see lane “E-500 mM maltose – Amyl. column”).

ZF NTnC was successfully purified after size exclusion column chromotography (Figure 3.2.2B: see lane “Sample input”; Figure 3.2.3B: see lane “Sample input”). Fractions containing pure ZF NTnC were used for ITC (Figure 3.2.2B and Figure 3.2.3B).

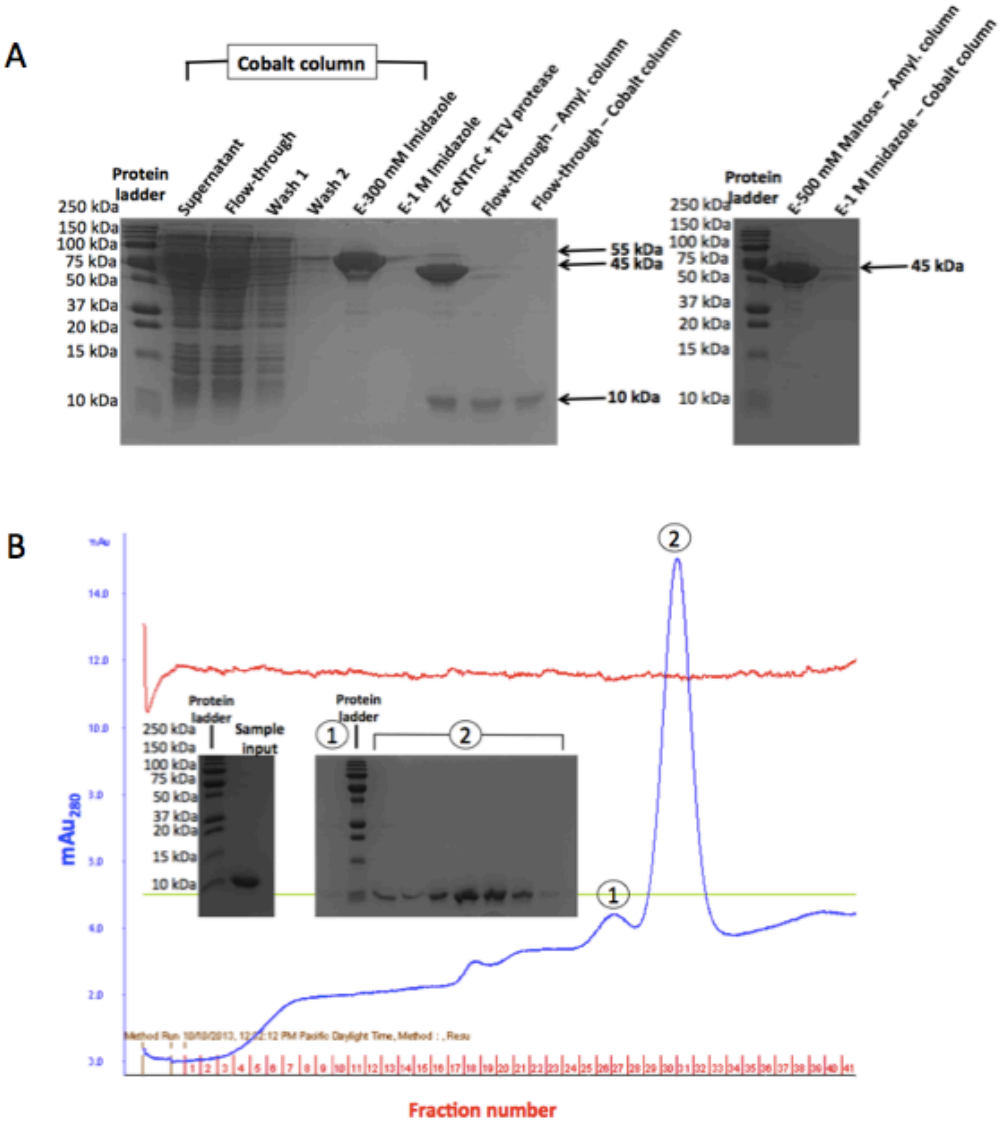

Figure 3.2.2 Purification of ZF cNTnC.
Samples of each purification step for ZF cNTnC were visualized by SDS-PAGE. A. Supernatants from 6-His-MBP ZF cNTnC were loaded onto a cobalt column. Wash 1 and 2 contains buffer with no imidizaole to remove unbound protein. "E-300 mM Imidazole" displays success of fusion protein (~55 kDa) binding to and elution from cobalt column. "ZF cNTnC + TEV protease" displays success of TEV protease cleavage indicated by a prominent band of the 6-His-MBP tag (~45 kDa) and ZF cNTnC (10 kDa). B. A chromatogram of ZF cNTnC from S100 column to remove larger molecular weight bands. Precision Plus Protein™ Unstained Standards (BioRad) were used as protein ladders.

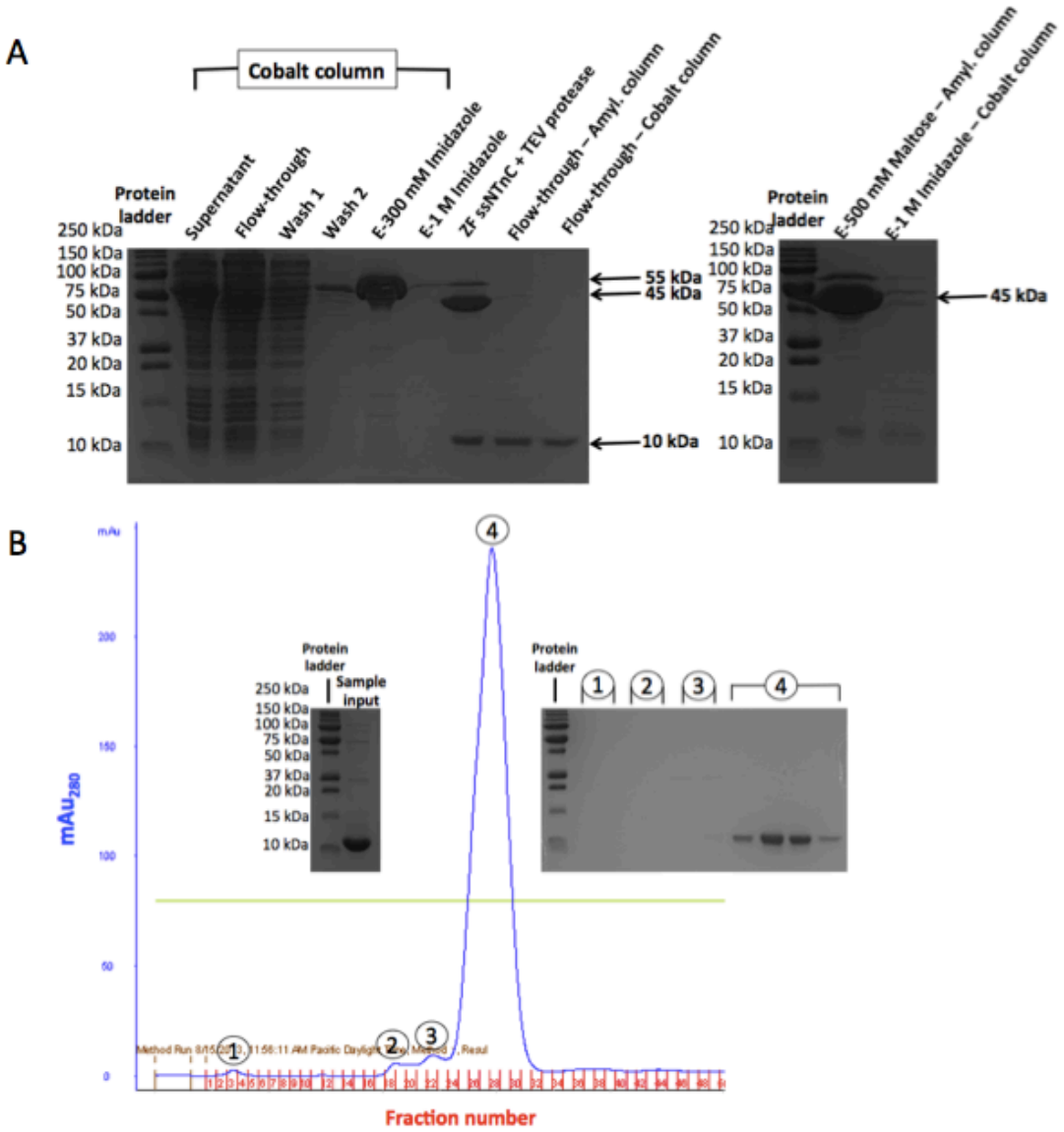

Figure 3.2.3 Purification of ZF ssNTnC

Samples of each purification step for ZF ssNTnC were visualized SDS-PAGE. A. Supernatants from 6-His-MBP ZF cNTnC were loaded onto a cobalt column. Wash 1 and 2 contains buffer with no imidizaole to remove unbound protein. “E-300 mM Imidazole” displays success of fusion protein (~55 kDa) binding to and elution from column. “ZF ssNTnC + TEV protease” displays success of TEV protease cleavage indicated by a prominent band of the 6-His-MBP tag (~45 kDa) and ZF ssNTnC (10 kDa). B. A chromatogram of ZF ssNTnC from S100 column to remove larger molecular weight bands. Purification of ZF ssNTnC was successful. Precision Plus Protein™ Unstained Standards (BioRad) were used as protein ladders.

3.2.2. Determining the Ca^{2+} binding properties in ZF cNTnC using isothermal titration calorimetry

ITC was used to determine the thermodynamic parameters between the ZF cNTnC and Ca^{2+} interaction. The experiments were done at three temperatures: 28°C, 18°C and 8°C. Endothermic reactions were observed in all three cases (Figure 3.2.4). Three replicates of ZF cNTnC and Ca^{2+} interaction were done at 28°C and 18°C. Two replicates of ZF cNTnC and Ca^{2+} interaction were done at 8°C. Background determinations were measured by titrating the ligand, Ca^{2+}, into buffer. The data were averaged and subtracted for each titration experiment.

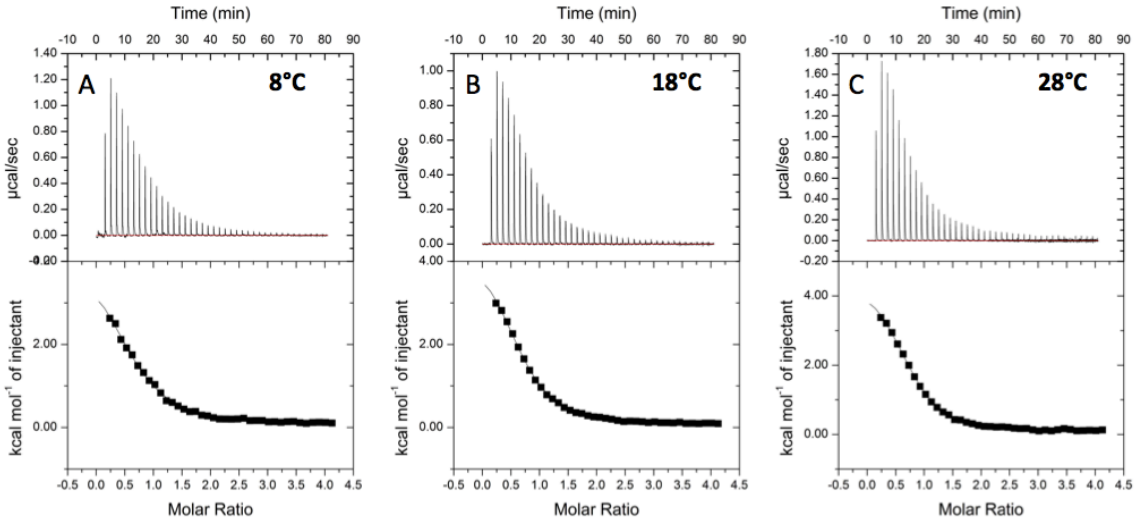

Figure 3.2.4 Characterization of ZF cNTnC using ITC
Binding interaction was observed upon Ca^{2+} titration into ZF cNTnC. A. Titration of Ca^{2+} (4 mM) into 200 µM ZF cNTnC performed at 8°C. 1 µL injections (40 injections total). B. Titration of Ca^{2+} (4 mM) into 200 µM ZF cNTnC performed at 18°C. 1 µL injections (40 injections total). C. Titration of Ca^{2+} (4 mM) into 200 µM ZF cNTnC performed at 28°C. 1 µL injections (40 injections total). (Top) Raw heats from titration of Ca^{2+} into ZF cNTnC. (Bottom) Integrated heats from titration of Ca^{2+} into ZF cNTnC. All experiments were performed on MicroCal iTC200 (GE Healthcare) instrument. For thermodynamic parameters determined, please see Table 3.2.1.

The average N values determined for cNTnC at 28°C, 18°C and 8°C were 0.70 ± 0.05, 0.68 ± 0.06, and 0.68 ± 0.01, respectively, suggesting a 1:1 molar ratio. Verification of the integrity of the sample following ITC revealed there were no aggregate or dimer formations. Only a single symmetrical peak was observed on the chromatogram (see Figure 3.2.5) indicating the absence of protein aggregate or dimer formation.

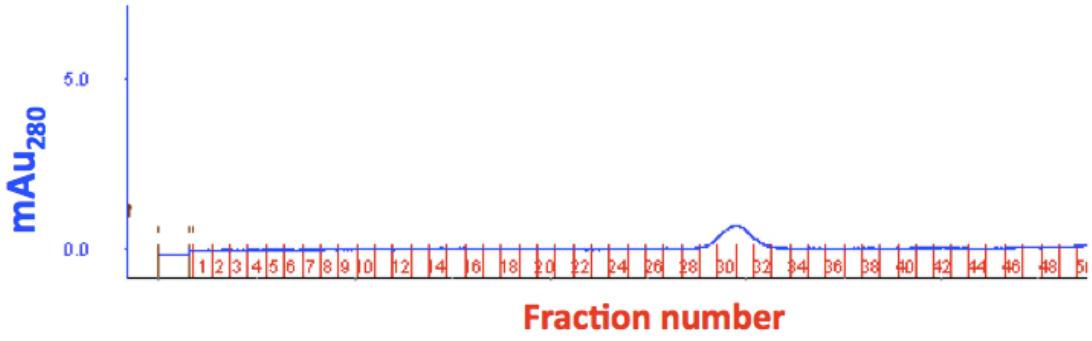

Figure 3.2.5 Size exclusion chromatogram of ZF cNTnC.
A single peak was observed indicating monomeric form of ZF cNTnC following ITC experiment.

The average and associated standard deviation for each thermodynamic parameter was determined (Table 3.2.1). The averaged binding affinities were converted to dissociation constants (K_d = 1/K_a). The dissociation constants, ΔH, ΔS and ΔG of cNTnC at 28°C, 18°C and 8°C are listed in Table 3.2.1.

Table 3.2.1 Thermodynamic parameters determined for ZF cNTnC and Ca^{2+} interaction at 8°C, 18°C and 28°C

	8°C	18°C	28°C
N*	0.68 ± 0.01	0.68 ± 0.06	0.70 ± 0.05
K_d (μM)*	53 ± 4	41 ± 8	24 ± 7
ΔH (cal/mol)*	4261 ± 104	4646 ± 356	4385 ± 269
ΔS (cal/mol/K)*	35.2 ± 0.7	36.1 ± 1	36.6 ± 1.0
TΔS (cal/mol)	9896 ±197	10507 ± 304	10781 ± 340
ΔG (cal/mol)	-5636 ± 93	-5862 ± 66	-6397 ± 110
Number of replicates	2	2	3

*Each parameter was determined using Origin 7 (OriginLab). The displayed values were calculated from taking the average and standard deviation of all replicates where: N is molar ratio; K_d is dissociation constant, ΔH is enthalpy, ΔS is entropy, and ΔG is Gibb's free energy. Determining the Ca^{2+} binding properties in ZF ssNTnC using isothermal titration calorimetry

ITC was used to determine the thermodynamic parameters between the ZF ssNTnC and Ca^{2+} interaction. Endothermic reactions were observed in all three cases indicting

binding of Ca^{2+} to ZF ssNTnC (Figure 3.2.6). Two replicates of ZF cNTnC and Ca^{2+} interaction was done at 28°C. Only one experiment at 18°C and 8°C were done.

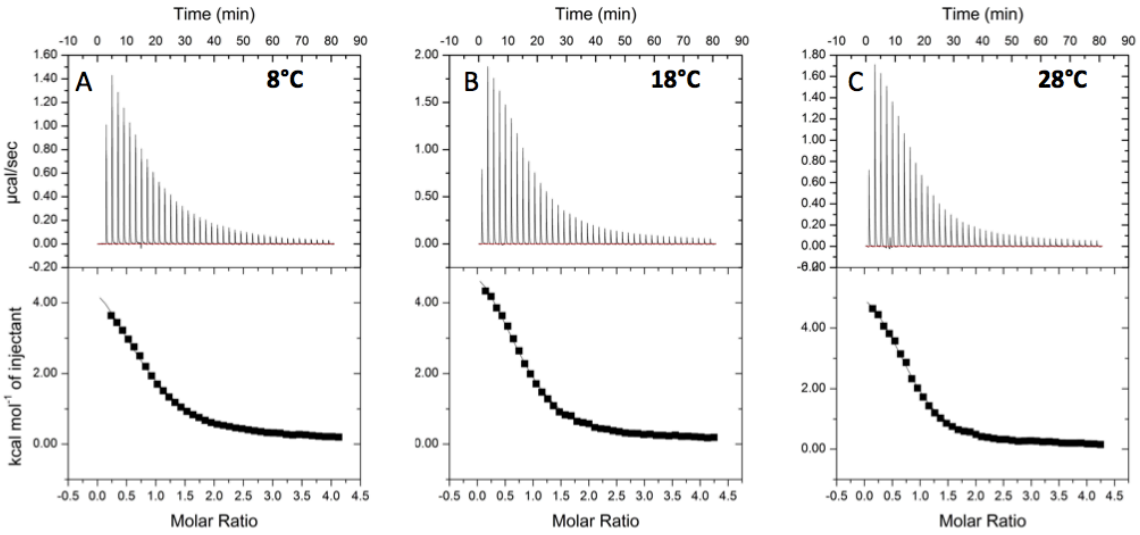

Figure 3.2.6 Characterization of ZF ssNTnC using ITC
Binding interaction was observed upon Ca^{2+} titration into ZF ssNTnC. A. Titration of Ca^{2+} (4 mM) into 200 µM ZF ssNTnC performed at 8°C. 1 µL injections (40 injections total). B. Titration of Ca^{2+} (4 mM) into 200 µM ZF ssNTnC performed at 18°C. 1 µL injections (40 injections total). C. Titration of Ca^{2+} (4 mM) into 200 µM ZF cNTnC (200 µM) performed at 28°C. 1 µL injections (40 injections total). (Top) Raw heats from titration of Ca^{2+} into ZF ssNTnC. (Bottom) Integrated heats from titration of Ca^{2+} into ZF ssNTnC. For thermodynamic parameters determined, please see Table 4.2.2.

The mean value for each thermodynamic parameter was calculated for titration experiments done at 28°C along with its associated standard deviation. The N value determined was 0.86 indicating a 1:1 molar ratio. The calculated averages for K_d, ΔH, ΔS and ΔG were 48 ± 6 µM, 6575 ± 422 cal/mol, 41.6 ± 1.2 cal/mol/K, -5938 ± 75 cal/mol, respectively (Table 4.2.2).

Table 3.2.2 Thermodynamic parameters determined for ZF ssNTnC and Ca^{2+} interaction at 8°C, 18°C and 28°C

	8°C	18°C	28°C
N	0.84 ± 0.03*	0.83 ± 0.02*	0.86 ± 0.02⬩
K_d (μM)	79 ± 5*	57 ± 3*	48 ± 6⬩
ΔH (cal/mol)	6160 ± 238*	6246 ± 172*	6575 ± 422⬩
ΔS (cal/mol/K)	40.7*	40.9*	41.6 ± 1.2⬩
TΔS (cal/mol)	11443	11908	12513 ± 346
ΔG (cal/mol)	-5283	-5662	-5938 ± 75⬩
Number of replicates	1	1	2

*Parameters were analysed using Origin 7 (OriginLab) where: N is molar ratio, K_d is dissociation constant, ΔH is enthalpy, ΔS is entropy, and ΔG is Gibb's free energy. Standard deviations displayed for N, K_d, and ΔH are associated with the deviation from the curve generated from integrating heat values.

⬩ The displayed values were calculated by taking the average and standard deviation of the two replicates.

The thermodynamic parameters for experiments done at 18°C and 8°C are listed in Table 4.2.2. The N-values determined for experiments done at 18°C and 8°C were 0.83 and 0.84, indicating a 1:1 molar ratio.

3.3. Site-directed mutagenesis and expression of full-length ZF cTnC and ssTnC

Success of the SDM procedure was confirmed by sequencing. Protein expression levels were visualized by SDS-PAGE. Bands were observed at molecular weight of approximately 18 kDa in lanes containing samples of IPTG-induced cultures. A negative control containing cultures grown in absence of IPTG was also loaded onto the 15% SDS-PAGE gel. The 18 kDa band was absent in these lanes (Figure 3.3.1).

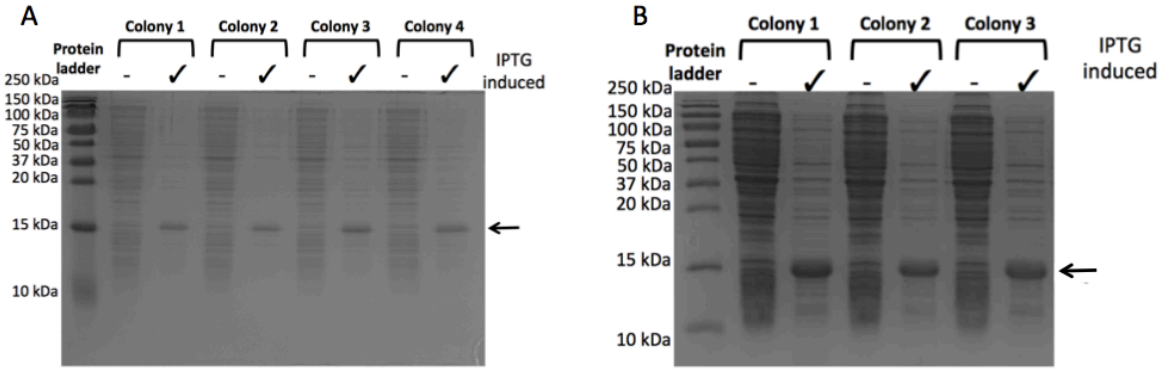

Figure 3.3.1 Expression of ZF cTnC and ssTnC after IPTG induction.
SDS-PAGE visualization of the protein expression test. Bands were observed at approximately 18 kDa. A. Expression of ZF cTnC. B. Expression of ZF ssTnC. (✓) indicates addition of IPTG. (-) indicates absence of IPTG. Prominent bands in IPTG induced lanes at approximately 18 kDa are indicated an arrow. Precision Plus Protein™ Unstained Standards (BioRad) were used as protein ladders.

3.3.1. Purification of full-length ZF cTnC

Fractions from each peak were collected and visualized by SDS-PAGE (Fig. 3.3.2). Pure ZF cTnC eluted from the DE52 column between 75 and 80% High Salt buffer concentration (Fig. 3.3.2).

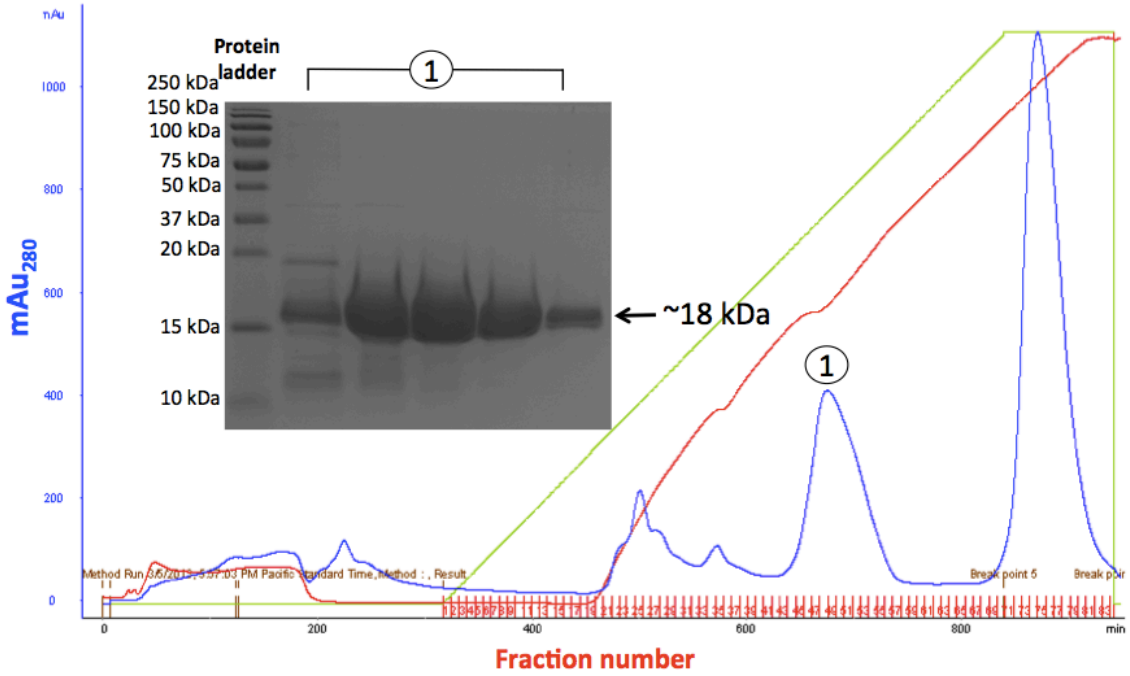

Figure 3.3.2 - Purification of ZF cTnC using DE52 (Sigma-Alderich) column.
Fractions under peak 1 (around 75 to 80% elution with 0.5 M KCl) were visualized on a 15% SDS-PAGE gel. cTnC was seen at the expected molecular weight of approximately 18 kDa. Pure ZF cTnC were collected for further experiments. The blue-line indicates UV absorbance at 280 nm. The green line indicates the linear gradient applied for 0.5 M KCl (High Salt buffer). The red line indicates the electrical conductivity. Precision Plus Protein™ Unstained Standards (BioRad) were used as protein ladder.

3.3.2. Purification of full-length ZF ssTnC

Fractions under each peak were visualized by SDS-PAGE (Fig. 3.3.3). Fractions containing pure ZF ssTnC were eluted between 75 and 80% of high salt buffer concentration (Fig. 3.3.3). Larger molecular weight bands were visible in the 15% SDS-PAGE gel in lanes containing ZF ssTnC. These fractions containing were pooled together and further purified by size exclusion chromatograph (Figure 3.3.4).

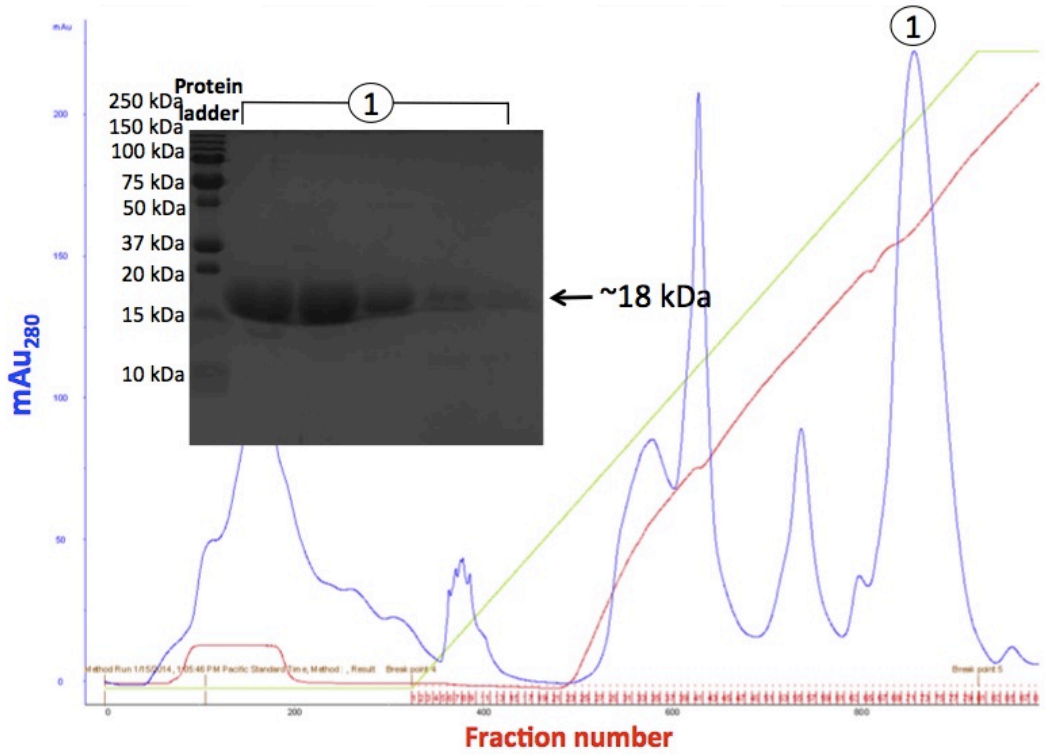

Figure 3.3.3 Purification of ZF ssTnC using a DEAE column (Sigma-Alderich)
Fractions under peak 1 (around 75 to 80% elution with 0.5 M KCl) were visualized on a 15% SDS-PAGE gel. ZF ssTnC was seen at the expected molecular weight of 18 kDa. The blue-line indicates UV absorbance at 280 nm. The green line indicates the linear gradient applied for 0.5 M KCl (High Salt buffer). The red line indicates the electrical conductivity. Precision Plus Protein™ Unstained Standards (BioRad) were used as protein ladders.

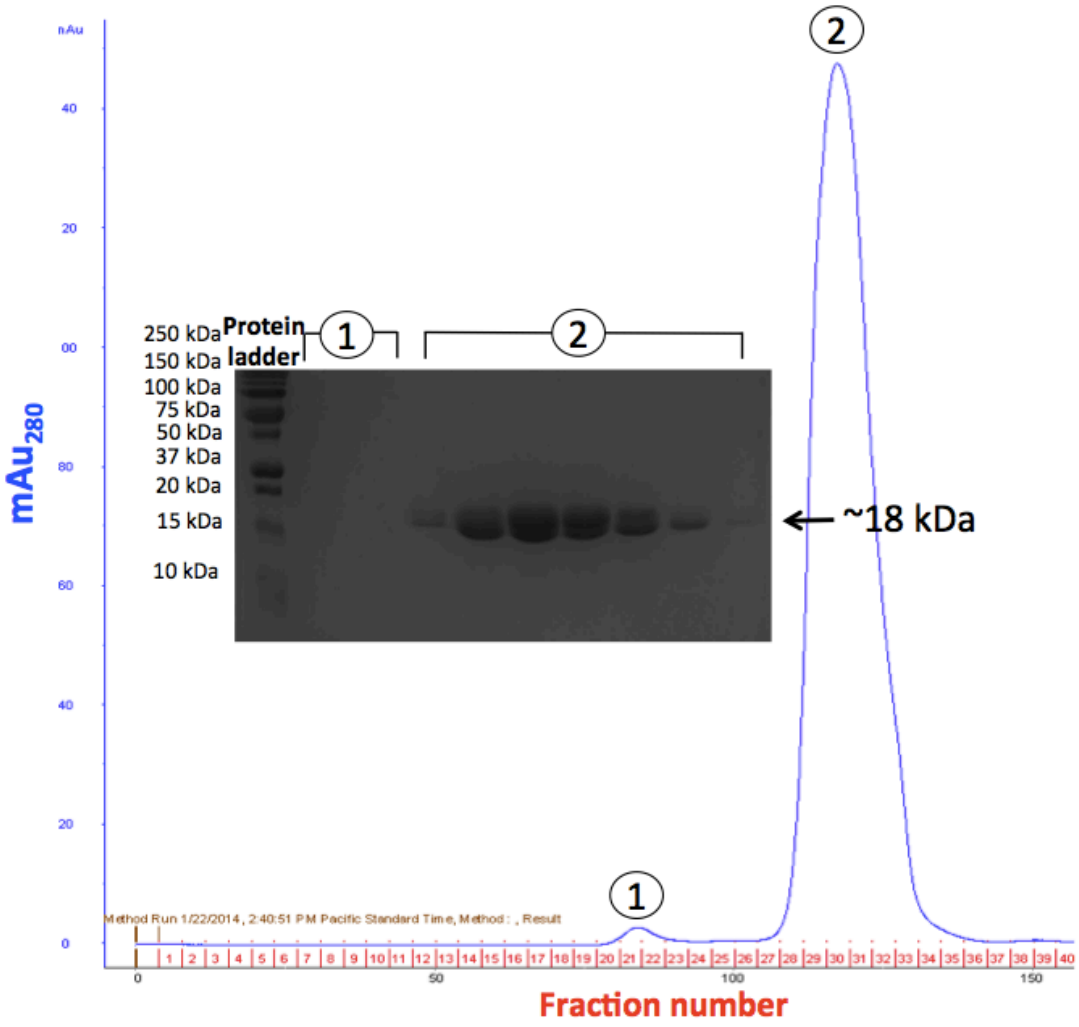

Figure 3.3.4 Further purification of ZF ssTnC using S-100 column
ZF ssTnC was further purified using Sephracryl-100 (GE Healthcare) column. Fractions under peaks 1 and 2 were visualized on a 15% SDS-PAGE gel. ZF ssTnC was seen in fractions under peak 2 at the expected molecular weight of 18 kDa. Precision Plus Protein™ Unstained Standards (BioRad) were used as protein ladders.

3.3.3. Determination of T_m for full-length Zebrafish cTnC and ssTnC

The T_m determined for ZF cTnC and ZF ssTnC were 57.0 ± 1.8°C and 54.6 ± 1.1°C, respectively with a p-value of 0.0004. ZF cTnC is only ~2°C slightly more stable than ZF ssTnC (Fig. 3.3.5).

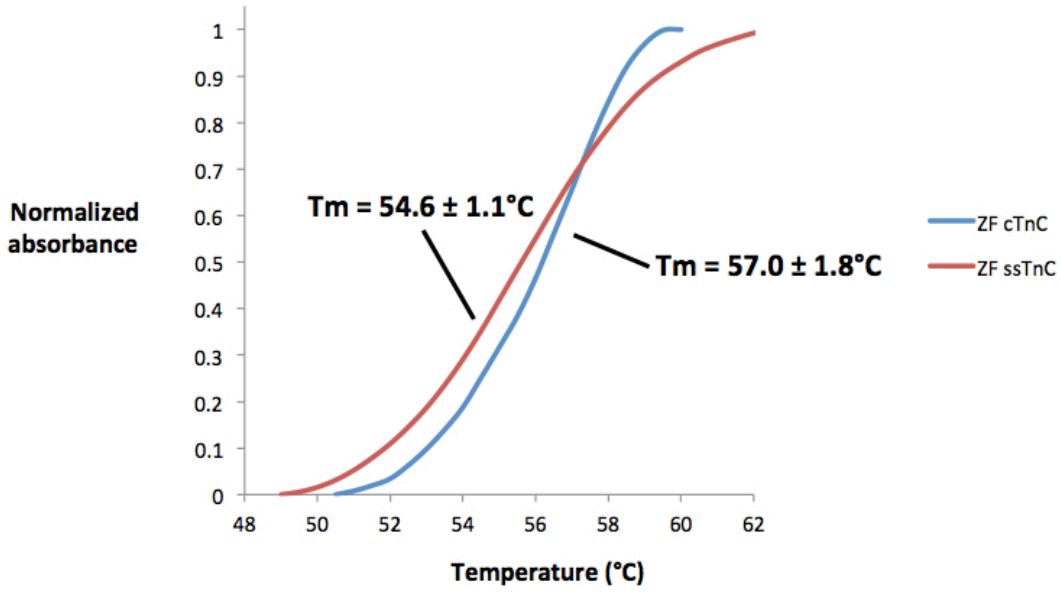

Figure 3.3.5 T_m temperatures of ZF cTnC and ssTnC.
The thermal stability determined for both ZF cTnC and ssTnC using Sypro Orange (Invitrogen). ZF cTnC had a Tm of 57.0 ± 1.8°C. ZF ssTnC had a Tm of 54.6 ± 1.1°C. Melting temperatures were determined by taking the maxima of the first derivative of each melting curve. *p-value* is less than 0.0004.

Chapter 4. Discussion

4.1. The binding affinities determined for ZF cNTnC and ssNTnC

The endothermic heat signals generated from the interactions observed between Ca^{2+} and ZF NTnC proteins demonstrate that ITC can be used to directly determine their binding affinities. The K_d values for each construct show an increase in binding affinity with increasing temperature. The ΔG calculated from each interaction also becomes more negative with increasing temperature, which indicates that the interaction is favoured at higher temperatures. The ΔH and ΔS determined for each ZF NTnC have similar values at all temperatures. In order for the interaction to be a favourable one, TΔS must be higher than that of ΔH. The only other factor influencing a higher TΔS is temperature (Tables 3.2.1 and 3.2.2). This implies that the Ca^{2+} and ZF NTnC interactions are entropic processes that are dependent on temperature.

ZF cNTnC has an overall higher affinity for Ca^{2+} in comparison to ZF ssNTnC. At 28°C, the Ca^{2+} dissociation constant (K_d) of cNTnC (24 ± 7 μM) is 2-fold higher than that of ssNTnC (48 ± 6 μM). At 18°C, cNTnC (41 ± 8 μM) is 1.5-fold higher than ssNTnC (57 μM ± 3). At 8°C, cNTnC (53 ± 4 μM) is 1.5-fold higher than ssNTnC (79 ± 5 μM). It is also important to note that the comparisons made between cNTnC and ssNTnC are based on a limited number of replicates done at each temperature. Future experiments need to include sufficient repeats for each ITC ZF NTnC experiment to make better comparisons.

The N-values ranged from 0.68 and to 0.70 for ZF cNTnC (Table 3.2.1) which is lower than expected (1.0). This may be explained, in part by the uncertainty in protein concentration measurements. The NTnC constructs contain only one tyrosine residue and the Edelhoch method was used to determine the protein concentration. This method

relies on the extinction coefficients of aromatic molecules and the absorbance measured at UV_{280} in denaturing buffer (Edelhoch 1967). However with a single tyrosine molecule in the NTnC molecule, the reading may become inaccurate due to the low extinction coefficient. If there were minute contaminants that cannot be visualized by SDS-PAGE or on a size exclusion chromatogram and contains many tryptophan and tyrosine residues, this would give a higher than actual reading of the cNTnC protein concentration. Future experiments may include MALDI-TOF experiments to determine the purity of the protein sample used. Bradford or Lowry colourimetric assays could also be used in the future to verify protein concentration (Olson and Markwell 2007). Three batches of ZF cNTnC were purified for all ZF cNTnC ITC experiments. In all cases, the N-value indicates that approximately only 70% of the protein is active. Thus another possibility for the lower N-value observed is that a fraction NTnC of the protein sample was improperly folded. This may affect the ability of site II to bind to Ca^{2+}. A possible solution is to use a different purifying method, such as a hydrophobic column in an attempt to improve the purity for functional protein.

ZF hearts displayed an overall higher expression of cTnC mRNA transcripts and this may be reflected by the higher affinity for Ca^{2+} required for cardiac muscle contraction in both chambers. At lower temperatures (18°C), cTnC mRNA transcripts are higher than that of ssTnC mRNA transcripts in both the atrium and ventricle (Genge, Davidson et al. 2013). The K_d value for cTnC at this temperature is 41 μM. At higher temperatures (28°C), ssTnC mRNA transcripts are 2-fold higher than that of cTnC in the atrium (Genge, Davidson et al. 2013). The K_d value for ssTnC at this temperature is 48 μM.

In both cases, it appears that certain transcripts are expressed at higher levels where the binding affinity is around 41 to 48 μM. As mentioned in section 1.2, the calcium influx through the L-type calcium channel in ZF ventricular cardiomyocytes displayed a higher $I_{Ca,L}$ current density than observed in mammalian species (section 1.2). This implies that the extracellular space through calcium channels on the cell membrane, rather than from the SR, is the source for increased cytosolic Ca^{2+} concentration for E-C coupling (Zhang, Llach et al. 2011). A higher expression of ZF ssTnC mRNA transcripts in the atrium and a 150-fold lower transcript level of cTnC in the ventricle may imply that a certain Ca^{2+} binding affinity is preferred for regulation of

muscle heart contraction at specific temperatures. This also suggests a teleological reason as to why ectotherms may turn the TnC paralog expression on and off to adapt to change in ambient temperature.

It is important to note that transcript expression level may not reflect the exact amount of functional protein being expressed in each chamber. Studies have shown that a mammalian cell, on average, produces two copies of mRNA per hour with a half-life ranging from 2.6 to 7 hours. Dozens of proteins can be expressed and made per hour with an average half-life of 46 hours (Vogel and Marcotte 2012).

Other studies have shown a higher Ca^{2+} binding affinity in mammalian cTnC and teleost cTnC than the binding affinities determined in this study. One such study employed F27W cTnC mutation to measure the emitted fluorescence upon Ca^{2+} titration. Trout cTnC (2.1 ± 0.3 μM) was shown to have a two-fold increase in binding affinity when compared to mammalian (bovine) cTnC (4.1± 0.5 μM) (Gillis, Marshall et al. 2000, Gillis, Moyes et al. 2003). There are four residues – Asn2, Ile28, Gln29, and Asp 30 (NIQD) – that distinguish teleost cTnC from mammalian cTnC. When the residues NIQD were substituted into mammalian cTnC, an increase in Ca^{2+} binding affinity of 1.9-fold was observed (Liang, Chung et al. 2008). The Ca^{2+} binding affinities determined in Gillis *et al.* and Liang *et al.* were higher than the affinities determined for ZF cNTnC and ssNTnC using ITC (Gillis, Moyes et al. 2003, Liang, Chung et al. 2008).

A recent study by Skowronsky *et al.* used ITC to determine the Ca^{2+} binding affinity for human cNTnC at 25°C (Skowronsky, Schroeter et al. 2013). The raw heat signals from the reaction were endothermic in nature of which are in agreement with the ZF NTnC ITC results presented in this thesis. The Ca^{2+} binding affinity determined from their experiments was 10 μM, approximately two- and five-fold higher than ZF cNTnC and ZF ssNTnC, respectively, at 28°C (Table 4.4.1). The reason for this observed difference may be due to the difference in buffer composition and protein concentration (Table 4.1.2) (Skowronsky, Schroeter et al. 2013). The ZF cNTnC and ssNTnC studies were conducted with 50 mM of HEPES and 150 mM of KCl. A higher concentration of salt may modify the Ca^{2+} binding affinity. The residue differences in ZF cNTnC (7 residues difference) and ZF ssNTnC (9 residues difference) compared to human cNTnC may also contribute to the difference in binding affinity. Future studies should include

comparing mammalian cNTnC and teleost NTnC (cNTnC and ssNTnC) Ca^{2+} binding properties under identical buffer compositions.

Table 4.1.1 Comparison of Ca^{2+} binding affinities of TnC conducted in absence of fluorescence labels.

Construct (temperature)	K_d (μM)	Method	Reference
ZF cNTnC (28°C)	24	ITC	this study
ZF cNTnC (18°C)	41	ITC	this study
ZF cNTnC (8°C)	53	ITC	this study
ZF ssNTnC (28°C)	48	ITC	this study
ZF ssNTnC (18°C)	57	ITC	this study
ZF ssNTnC (8°C)	79	ITC	this study
Human cNTnC (25°C)	10	ITC	Skowronsky *et al.*
Human cTnC (4°C)	10	Equilibrium dialysis	Holroyde *et al.*

Table 4.1.2 Comparison of thermodynamic parameters and buffer composition of ITC studies of ZF NTnC and human cNTnC.

	ZF cNTnC	ZF ssNTnC	Human cNTnC
N*	0.70 ± 0.05	0.86 ± 0.02[w]	0.96 ± 0.01
Temperature (°C)	28	28	25
K_d (μM)*	24 ± 7	48 ± 6[w]	10 ± 1.9
ΔH (cal/mol)*	4385 ± 269	6575 ± 422[w]	3240 ± 200
TΔS (cal/mol)	10781 ± 340	12513 ± 346	10100 ± 220
ΔG (cal/mol)	-6397 ± 110	-5938 ± 75[w]	-6830 ± 110
Protein concentration (μM)	200 or 100	200	40 to 70
Buffer composition	50 mM HEPES, pH 7.2 150 mM KCl 10 mM 2-β-mercaptoethanol	50 mM HEPES, pH 7.2 150 mM KCl 10 mM 2-β-mercaptoethanol	10 mM MES, pH 7.0 50 mM KCl
Reference	This study.	This study.	(Skowronsky, Schroeter et al. 2013)

The difference in Ca^{2+} binding affinities observed in previous teleost and mammalian studies may be contributed by differences in techniques and species of TnC used. Holroyde *et al.* determined the Ca^{2+} binding affinity for bovine cTnC to be 10 μM using traditional equilibrium dialysis and $^{45}CaCl_2$ (Table 3.3.1) (Holroyde, Robertson et al. 1980) at 4°C. Subsequent studies used covalent attachment of fluorescence labels to certain residues of cTnC to determine the Ca^{2+} binding affinity of site II (please refer to section 1.7 for further details). Many of these labels are bulky and may jeopardize the structural and functional integrity of the molecule. All fluorescence labels used to date react with thiol groups with the exception of the F27W mutation in cTnC. cTnC has two cysteine residues at position 35 and 84. Studies have either mutated one or both of cysteines to attach a fluorophore at either or both sites (Putkey, Liu et al. 1997, Tikunova and Davis 2004, Wang, Robertson et al. 2012). More recent studies also mutated both cysteines to serines and introduced a Thr53Cys mutation. The purpose of this mutation was to better measure the fluorescence signal of Ca^{2+} binding to site II of cTnC. Avoiding

fluorophore attachment at Cys84 also would reduce the potential interfering effects of cTnC-cTnI interaction (Tikunova and Davis 2004, Li, Stevens et al. 2013). It is important to note that the additive effects from covalent attachment and mutations can jeopardize the accuracy for determining the Ca^{2+} binding properties of the regulatory site of cTnC. Furthermore, the fluorescent label, IAANS, is a fairly commonly used label to attach to the Cys84 residue for determining the Ca^{2+} binding affinity of cTnC. A recent study showed that C84Y mutation was found in a patient with HCM and therefore, implicates that this residue has a structural or functional role (Landstrom, Parvatiyar et al. 2008, Pinto, Parvatiyar et al. 2009).

4.2. The melting temperatures determined for ZF cTnC and ssTnC

The difference in melting temperatures between ZF cTnC and ssTnC was not large enough to explain why chamber-specific and differential expression was observed in the ZF heart (Genge, Davidson et al. 2013). ZF can survive at temperatures ranging from 6°C to 38°C with the optimal temperature being ~28°C. The T_m of 57.0 ± 1.8°C and 54.6 ± 1.1°C determined for both cTnC and ssTnC, respectively, were well beyond their temperature threshold. Although these values are significantly different from each other (*p-value* < 0.0004), cTnC is only slightly more stable than ssTnC with a melting temperature 2°C higher.

However, it is known that knocking down either gene using *tnnc1a* or *tnnc1b* morpholinos impairs ventricle contractility, ventricular morphology and atrium contractility in the embryonic ZF (see section 1.3) (Sogah, Serluca et al. 2010). This strongly suggests that both genes are essential for the proper functioning of the two chambers in ZF heart. Further experiments are needed to further investigate the relation between the differential-expression at various temperatures observed in each chamber.

Other studies have employed CD spectroscopy to look at any structural changes in terms of α-helical content in disease-associated cTnC mutants. Several mutations found in cTnC including A8V, C84Y, D145E, A23Q, V44Q, E40Q and I61Q showed increase or decrease in α-helical content, in comparison to wild type cTnC, under

various or Mg^{2+} or Ca^{2+} conditions. The increase or decrease in α-helical content may be a good indication to an increased or decreased stability of the protein respectively. The data imply that the structural properties of mutant cTnCs may alter the binding affinity towards Ca^{2+} and thereby lead to subsequent heart disease.

Chapter 5. Summary/Future Directions

This study used ITC to directly measure the Ca^{2+} binding affinities of ZF NTnC. No fluorescent labels were required in the process. Previous ITC studies also displayed endothermic heat signals of which are in agreement with ZF NTnC studies in this study. The Ca^{2+} binding affinities determined for ZF NTnC are two to five fold lower in binding affinity when compared to the values determined by Holroyde *et al.* and Skowronsky *et al.* This may be due the techniques used and the experimental conditions that were used to determine the binding affinities. Further studies conducted under the same buffer composition and temperatures would be required to do a proper comparison study of Ca^{2+} binding affinity between mammalian and teleost NTnC.

Future directions include increasing the number of titration experiments with ZF cNTnC/ssNTnC at 28°C, 18°C and 8°C to ensure reproducibility of results and to test for significant difference. Only the averages were calculated for titrations that were replicated more than once. Whether the affinities between temperatures of the same protein or between different proteins were significantly different could not be determined because some experiments were only done once.

Future experiments should also include determining the Ca^{2+} binding affinity of ZF NTnCs in the presence of Mg^{2+}. All titration experiments conducted in this thesis were done in the absence of Mg^{2+}. Mg^{2+} is present in the cytosol of virtually all teleost and mammalian cells at a concentration of about 1 mM. Determining the Ca^{2+} binding affinity of ZF NTnC under these concentrations may closer reflect the true Ca^{2+} binding affinity under physiological conditions. Preliminary studies of wild-type human cNTnC were done and showed that Ca^{2+} does indeed displace Mg^{2+}. Please refer to Appendix A for further details.

The T_m for ZF cTnC and ssTnC were determined with ZF cTnC being slightly more stable than ZF ssTnC. Experiments were done under Ca^{2+}-free conditions. Experiments by previous studies using CD spectroscopy showed increased α-helical

content upon addition of Ca^{2+} to the solution. Future experiments should include determining the T_m for each protein under Ca^{2+}/Mg^{2+}-saturated conditions to see if a difference in T_m would be observed.

Appendix A.

Preliminary studies using ITC to determine the Ca^{2+} binding affinity of wild-type human cNTnC and L29Q cNTnC

Introduction

L29Q cTnC is associated with familial hypertrophic cardiomyopathy (FHC). FHC is characterized by asymmetrical hypertrophy, myocardial disarray, contractile dysfunction and arrhythmias. FHC-causing mutations can lead to impaired calcium cycling and sensitivity, and altered myofilament length-dependent activation (Frey, Luedde et al. 2012). L29Q is the first mutation identified in cTnC to cause FHC (Hoffmann, Schmidt-Traub et al. 2001). Studies show both L29Q cTnC displaying an increase in Ca^{2+}-binding affinity while other studies also show no significant difference in Ca^{2+}-binding affinity in comparison to wild-type cTnC. Under β-adrenergic stimulation conditions, serine residues 23 and 24 of cTnI are phosphorylated by protein kinase A (PKA). Peptide studies show that the N-terminal arm of cTnI, which include the phosphorylation sites (Ser23/24), interacts with the N-terminal region of cTnC. Mutation of residue 29 to a glutamine appears to alter this interaction and thereby hinder the transfer of the phosphorylation signal from cTnI to cTnC during β-adrenergic stimulation (Finley, Abbott et al. 1999, Schmidtmann, Lindow et al. 2005).

Studies to determine the affinity of Ca^{2+} binding to site II of WT and L29Q cTnC have been done on either the full-length or N-lobe only (cNTnC; residues 1 to 89) constructs. All previous studies use fluorescence labels that have been incorporated into the protein to determine the metal binding affinities towards cTnC. These labels include IAANS at cysteine residue 35, 84 or both (Davis, Norman et al. 2007, Dweck, Hus et al. 2008). IAANS label is also used at residue 53 of cTnC by mutating this residue from a threonine into a cysteine and eliminating cysteines at residues 35 and 84. Other methods for determining binding affinities also include introducing a tryptophan at position 27 (F27W) and measure the emitted wavelength of 330 nm upon Ca^{2+} titration (Liang, Chung et al. 2008).

We hypothesize that the L29Q cNTnC will display a high Ca^{2+} binding affinity in comparison to wild-type cNTnC. The objectives for this study were to determine and compare the Ca^{2+} binding affinity of wild-type and L29Q cNTnC determined by ITC.

Materials and Methods

For expression of wild-type and L29Q cTnC proteins, each construct was transformed into BL21 (DE3) cells. Transformed BL21 (DE3) cells were grown in 100 mL of LB with ampicillin (100 µg/mL final concentration) overnight for approximately 16 hours in a shaker at 37°C with shaking at 250 rpm. 10 mL of overnight culture were inoculated into 1 L of LB with ampicillin. The culture was incubated for 3 hours at 37°C with shaking at 250 rpm. Protein production was then induced with isopropyl β-D-1-thiogalactopyranoside (IPTG) to a final concentration of 1 mM. Cells were incubated to grow for a further 3 hours at 37°C with shaking at 250 rpm. Cells were then harvested by centrifugation at 6000 x g for 10 minutes at 4°C. Supernatant was discarded and the pellet was stored at -80°C.

The pellet from one litre of culture was resuspended in 30 mL of cold Resuspension Buffer (50 mM Tris, pH 7.5, 0.05 M NaCl, 1mM DTT, 1 mM PMSF and 1 complete protease inhibitor tablet (Roche). The cell suspension was placed on ice and lysed by sonication with 4 or 5 pulses at 80% amplitude for 20 seconds per pulse. The cell lysate was then centrifuged at 14,000 rpm in a Beckman JA17 rotor for 30 minutes at 4°C. The lysate supernatant was decanted. The sample was then filtered (0.45 µM syringe filter; Whatman) and warmed to room temperature. The sample was then loaded onto either a DE52 (Sigma-Alderich) anion exchange column at room temperature. The protein was eluted with High Salt Tris Buffer (25 mM Tris, pH 8.0, 550 mM NaCl, 1 mM EDTA and 14 mM BME). Fractions containing pure protein of interest were pooled together and transferred into dialysis tubing (MWCO: 3, 000 Da) and was dialyzed 5 times (at least overnight three times) against Tris Buffer (50 mM Tris, pH 8.0, 1 mM EDTA and 14 mM BME) at 4°C. Protein was then applied onto a DEAE (GE Healthcare) column for further purification. The NTnC proteins were subsequently purified by size exclusion chromatography using a HiPrep 26/60 Sephracryl S-100 (GE Healthcare) column. The sample was then concentrated and dialyzed against 2 L of HEPES Buffer

(50 mM HEPES, pH 7.2, 150 mM KCl and 10 mM BME) at least five-times. Purified proteins were stored at -80°C.

The Edelhoch method was used to determine protein concentration. Please see section 2.5.2 for details.

ITC was done on human cNTnC constructs. All ITC experiments were performed on a MicroCal iTC200 (GE Healthcare) instrument. Experiments were conducted with 500 μM of ZF NTnC and 2 μL injections (20 injections in total) of 5 mM Ca^{2+}/Mg^{2+} with 120 seconds spacing at 1000 rpm. Experiments were performed at 25°C.Origin 7.0 (OriginLab) was used to analyze binding isotherms.

Preliminary results

Wild-type and L29Q cNTnC were obtained from purification procedures. Purity was confirmed by SDS-PAGE. L29Q cNTnC contained higher molecular weight bands and was applied to a size exclusion column. Fractions containing pure protein were visualized using SDS-PAGE.

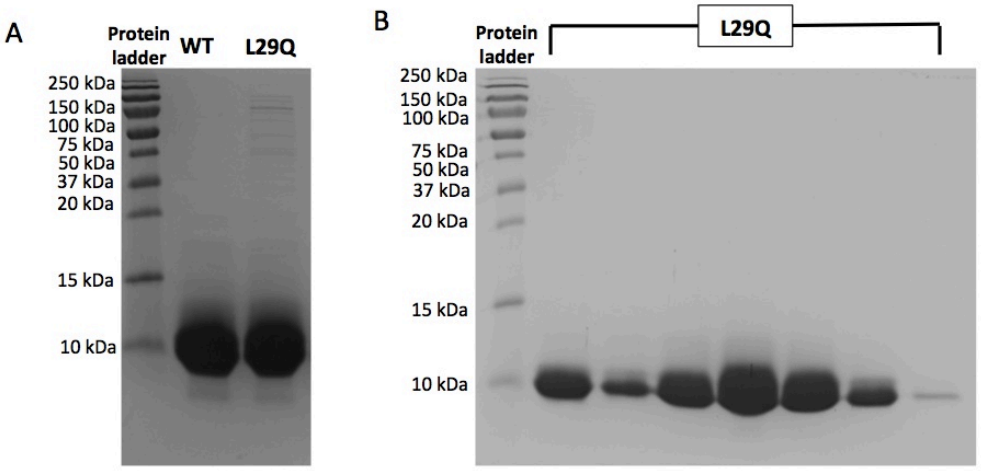

Figure A 1 15% SDS-PAGE of wild-type and L29Q cNTnC
Concentration of wild-type (WT) and L29Q cNTnC were visualized by SDS-PAGE analysis to confirm purity of protein sample. A. WT cNTnC and L29Q cNTnC. Higher molecular weight bands are observed in lane containing L29Q cNTnC. B. Fractions of L29Q cNTnC were collected from Sepharcryl 100 (GE Healthcare) column and visualized by SDS-PAGE to confirm purity. Precision Plus Protein™ Unstained Standards (BioRad) were used as protein ladder.

ITC was used to determine the Ca^{2+} binding interaction of wild-type cNTnC and L29Q cNTnC. The thermodynamic parameters with their standard deviations from the curve are listed in Table A1. Endothermic reactions were observed for both cases (Figure A2).

Table A 1 Thermodynamic parameters determined for WT cNTnC and L29Q cNTnC Ca^{2+} interaction

	WT cNTnC	L29Q cNTnC
N	0.68 ± 0.021	0.92 ± 0.0082
K_d (μM)	29 ± 6.1	25.6 ± 1.6
ΔH (cal/mol)	3355± 143	2804 ± 0
ΔS (cal/mol/K)	32.0	30.4
ΔG (cal/mol)	-6186	-6260

Parameters were analyzed using Origin 7 (OriginLab) where: N is molar ratio, K_d is dissociation constant, ΔH is enthalpy, ΔS is entropy, and ΔG is Gibb's free energy. Titrations done at 25°C: n = 1. Standard deviations displayed for N, K_d, and ΔH are associated with the deviation from the curve generated from integrated heat values.

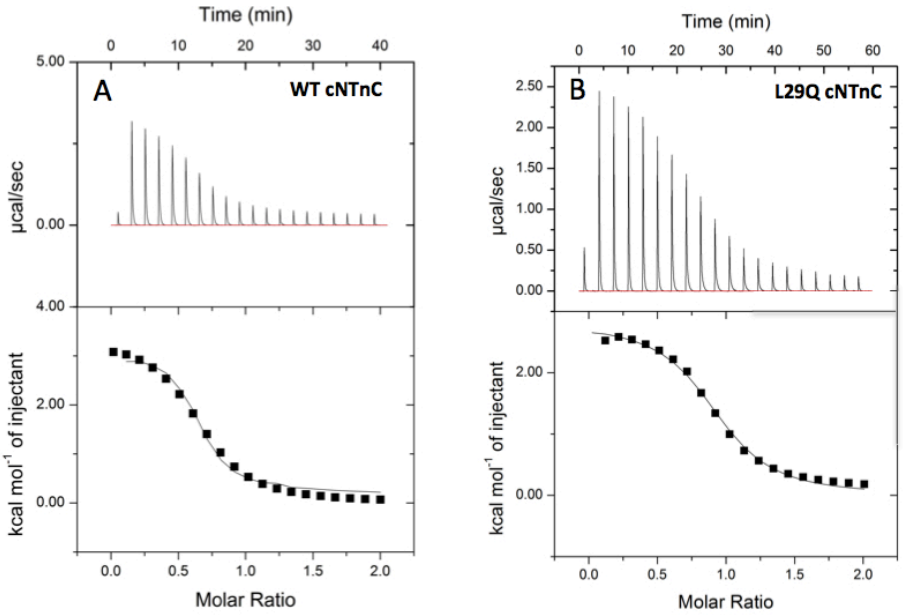

Figure A 2 Characterization of wild-type (WT) and L29Q cNTnC.
Endothermic reactions were observed upon Ca^{2+} titration into WT and L29Q cNTnC. A. Titration of Ca^{2+} (5 mM) into 500 μM WT cNTnC performed at 25°C. 2 μL injections (20 injections total). B. Titration of Ca^{2+} (5 mM) into 500 μM L29Q cNTnC performed at 25°C. 2 μL injections (20 injections total). (Top) Raw heats from titration of Ca^{2+} into cNTnC. (Bottom) Integrated heats from titration of Ca^{2+} into cNTnC. For thermodynamic parameters determined, please see Table A1.

An interaction between Mg^{2+} and wild-type cNTnC was observed using ITC. The heat signals were weak. Therefore, the thermodynamic parameters could not be determined. A weak endothermic reaction was observed (Figure A 3B). Mg^{2+} was also titrated into buffer. The background control gave slight exothermic heat signals, which confirms that Mg^{2+} is interacting weakly with wild-type cNTnC (Figure A 3A).

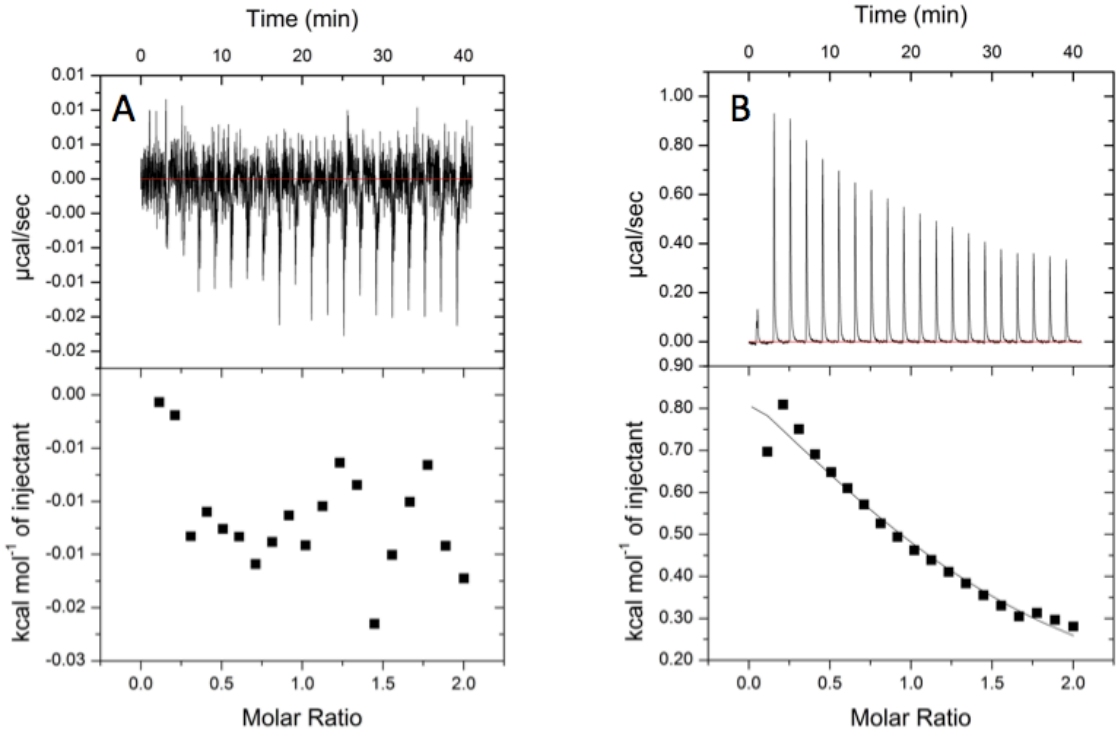

Figure A 3 Weak interaction observed between Mg^{2+} and wild-type (WT) cNTnC. A weak endothermic reaction was observed upon Mg^{2+} titration into WT cNTnC. A. Titration of Mg^{2+} (5 mM) into HEPES buffer performed at 25°C. 2 µL injections (20 injections total). B. Titration of Mg^{2+} (5 mM) into 500 µM WT cNTnC performed at 25°C. 2 µL injections (20 injections total). (Top) Raw heats from titration of Ca^{2+} into cNTnC. (Bottom) Integrated heats from titration of Ca^{2+} into cNTnC.

Discussion

Preliminary ITC results show that the Ca^{2+} binding affinity of wild-type and L29Q cNTnC can be determined. Endothermic reactions were observed for both reactions. The thermodynamic parameters determined for wild-type cNTnC is not accurate because the curve could not be fitted to the integrated heat values (Figure A 3). The N-value of 0.682 is also lower than the expected. Matrix-assisted laser desorption/ionization – time of flight (MALDI-TOF) was performed on wild-type cNTnC

sample (data not shown). A peak indicating the presence of wild-type cNTnC at 10 kDa was observed. A contaminant protein was also observed at approximately 8 kDa. This may have contributed to the low N-value observed from ITC and may explain why the curve did not fit well to the integrated heat values. ITC experiments conducted on L29Q cNTnC showed a clear endothermic reaction with Ca^{2+}. The curve also fitted well to the integrated heats with an N-value of 0.92. This indicates that Ca^{2+} is reacting in a 1:1 ratio. The Ca^{2+} binding affinity of L29Q cNTnC (25.6 μM) is slightly higher than that of wild-type cNTnC (29 μM). However, ITC experiments for wild-type cNTnC will need to be optimized for better curve fitting and ultimately to give more accurate results. Further ITC experiments for both proteins will be required to ensure the reproducibility of the results.

An interaction between Mg^{2+} and wild-type cNTnC was observed (Figure A 3). This interaction has never been observed before. This suggests that Ca^{2+} needs to displace Mg^{2+} at site II of cNTnC and would also mean a different binding affinity for Ca^{2+} would be observed.

Future directions

Further ITC experiments need to be conducted to determine the Ca^{2+} binding affinity for both wild-type and L29Q cNTnC in the presence and absence of Mg^{2+}. Because an interaction was observed between wild-type cNTnC and Mg^{2+}, a different Ca^{2+} binding affinity would be expected.

References

Ammash, N. M., J. B. Seward, K. R. Bailey, W. D. Edwards and A. J. Tajik (2000). "Clinical profile and outcome of idiopathic restrictive cardiomyopathy." Circulation **101**(21): 2490-2496.

Artimo, P., M. Jonnalagedda, K. Arnold, D. Baratin, G. Csardi, E. de Castro, S. Duvaud, V. Flegel, A. Fortier, E. Gasteiger, A. Grosdidier, C. Hernandez, V. Ioannidis, D. Kuznetsov, R. Liechti, S. Moretti, K. Mostaguir, N. Redaschi, G. Rossier, I. Xenarios and H. Stockinger (2012). "ExPASy: SIB bioinformatics resource portal." Nucleic Acids Res **40**(Web Server issue): W597-603.

Aslanidis, C. and P. J. de Jong (1990). "Ligation-independent cloning of PCR products (LIC-PCR)." Nucleic Acids Res **18**(20): 6069-6074.

Bers, D. M. (2002). Excitation-Contraction Coupling and Cardiac Contractile Force. Dordrecht, The Netherlands, Kluwer Academic Publishers.

Bill, B. R., A. M. Petzold, K. J. Clark, L. A. Schimmenti and S. C. Ekker (2009). "A primer for morpholino use in zebrafish." Zebrafish **6**(1): 69-77.

Bodi, I., G. Mikala, S. E. Koch, S. A. Akhter and A. Schwartz (2005). "The L-type calcium channel in the heart: the beat goes on." J Clin Invest **115**(12): 3306-3317.

Davis, J. P., C. Norman, T. Kobayashi, R. J. Solaro, D. R. Swartz and S. B. Tikunova (2007). "Effects of thin and thick filament proteins on calcium binding and exchange with cardiac troponin C." Biophys J **92**(9): 3195-3206.

Delano, W. L. (2002). The PyMOL Molecular Graphics System. San Carlos, Ca., Delano Scientific.

Di Maio, A. and B. A. Block (2008). "Ultrastructure of the sarcoplasmic reticulum in cardiac myocytes from Pacific bluefin tuna." Cell Tissue Res **334**(1): 121-134.

Dong, W. J., J. Xing, Y. Ouyang, J. An and H. C. Cheung (2008). "Structural kinetics of cardiac troponin C mutants linked to familial hypertrophic and dilated cardiomyopathy in troponin complexes." J Biol Chem **283**(6): 3424-3432.

Dweck, D., N. Hus and J. D. Potter (2008). "Challenging current paradigms related to cardiomyopathies. Are changes in the Ca2+ sensitivity of myofilaments containing cardiac troponin C mutations (G159D and L29Q) good predictors of the phenotypic outcomes?" J Biol Chem **283**(48): 33119-33128.

Edelhoch, H. (1967). "Spectroscopic determination of tryptophan and tyrosine in proteins." Biochemistry **6**(7): 1948-1954.

Ericsson, U. B., B. M. Hallberg, G. T. Detitta, N. Dekker and P. Nordlund (2006). "Thermofluor-based high-throughput stability optimization of proteins for structural studies." Anal Biochem **357**(2): 289-298.

Finley, N., M. B. Abbott, E. Abusamhadneh, V. Gaponenko, W. Dong, G. Gasmi-Seabrook, J. W. Howarth, M. Rance, R. J. Solaro, H. C. Cheung and P. R. Rosevear (1999). "NMR analysis of cardiac troponin C-troponin I complexes: effects of phosphorylation." FEBS Lett **453**(1-2): 107-112.

Frey, N., M. Luedde and H. A. Katus (2012). "Mechanisms of disease: hypertrophic cardiomyopathy." Nat Rev Cardiol **9**(2): 91-100.

Freyer, M. W. and E. A. Lewis (2008). "Isothermal titration calorimetry: experimental design, data analysis, and probing macromolecule/ligand binding and kinetic interactions." Methods Cell Biol **84**: 79-113.

Genge, C. E., W. S. Davidson and G. F. Tibbits (2013). "Adult teleost heart expresses two distinct troponin C paralogs: cardiac TnC and a novel and teleost-specific ssTnC in a chamber- and temperature-dependent manner." Physiol Genomics **45**(18): 866-875.

Gillis, T. E., C. R. Marshall, X. H. Xue, T. J. Borgford and G. F. Tibbits (2000). "Ca(2+) binding to cardiac troponin C: effects of temperature and pH on mammalian and salmonid isoforms." Am J Physiol Regul Integr Comp Physiol **279**(5): R1707-1715.

Gillis, T. E., C. D. Moyes and G. F. Tibbits (2003). "Sequence mutations in teleost cardiac troponin C that are permissive of high Ca2+ affinity of site II." Am J Physiol Cell Physiol **284**(5): C1176-1184.

Gordon, A. M., E. Homsher and M. Regnier (2000). "Regulation of contraction in striated muscle." Physiol Rev **80**(2): 853-924.

Gouet, P., X. Robert and E. Courcelle (2003). "ESPript/ENDscript: Extracting and rendering sequence and 3D information from atomic structures of proteins." Nucleic Acids Res **31**(13): 3320-3323.

Gusev, N. B. and N. V. Barskaya (1984). "Investigation of cation-binding properties of cardiac troponin C peptides by circular-dichroism spectroscopy." Biochem J **220**(1): 315-320.

Hoffmann, B., H. Schmidt-Traub, A. Perrot, K. J. Osterziel and R. Gessner (2001). "First mutation in cardiac troponin C, L29Q, in a patient with hypertrophic cardiomyopathy." Hum Mutat **17**(6): 524.

Holroyde, M. J., S. P. Robertson, J. D. Johnson, R. J. Solaro and J. D. Potter (1980). "The calcium and magnesium binding sites on cardiac troponin and their role in the regulation of myofibrillar adenosine triphosphatase." J Biol Chem **255**(24): 11688-11693.

Hove-Madsen, L., A. Llach, G. F. Tibbits and L. Tort (2003). "Triggering of sarcoplasmic reticulum Ca2+ release and contraction by reverse mode Na+/Ca2+ exchange in trout atrial myocytes." Am J Physiol Regul Integr Comp Physiol **284**(5): R1330-1339.

Hove-Madsen, L., A. Llach and L. Tort (2000). "Na(+)/Ca(2+)-exchange activity regulates contraction and SR Ca(2+) content in rainbow trout atrial myocytes." Am J Physiol Regul Integr Comp Physiol **279**(5): R1856-1864.

Hove-Madsen, L., C. Prat-Vidal, A. Llach, F. Ciruela, V. Casado, C. Lluis, A. Bayes-Genis, J. Cinca and R. Franco (2006). "Adenosine A2A receptors are expressed in human atrial myocytes and modulate spontaneous sarcoplasmic reticulum calcium release." Cardiovasc Res **72**(2): 292-302.

Huang, J., L. Hove-Madsen and G. F. Tibbits (2005). "Na+/Ca2+ exchange activity in neonatal rabbit ventricular myocytes." Am J Physiol Cell Physiol **288**(1): C195-203.

Icardo, J. M. (2012). The Teleost Heart: A Morphological Approach, Springer Science.

Kelly, S. M., T. J. Jess and N. C. Price (2005). "How to study proteins by circular dichroism." Biochim Biophys Acta **1751**(2): 119-139.

Kelly, S. M. and N. C. Price (2000). "The use of circular dichroism in the investigation of protein structure and function." Curr Protein Pept Sci **1**(4): 349-384.

Landstrom, A. P., M. S. Parvatiyar, J. R. Pinto, M. L. Marquardt, J. M. Bos, D. J. Tester, S. R. Ommen, J. D. Potter and M. J. Ackerman (2008). "Molecular and functional characterization of novel hypertrophic cardiomyopathy susceptibility mutations in TNNC1-encoded troponin C." J Mol Cell Cardiol **45**(2): 281-288.

Leavis, P. C. and E. L. Kraft (1978). "Calcium binding to cardiac troponin C." Arch Biochem Biophys **186**(2): 411-415.

Leavis, P. C., S. S. Rosenfeld, J. Gergely, Z. Grabarek and W. Drabikowski (1978). "Proteolytic fragments of troponin C. Localization of high and low affinity Ca2+ binding sites and interactions with troponin I and troponin T." J Biol Chem **253**(15): 5452-5459.

Leavitt, S. and E. Freire (2001). "Direct measurement of protein binding energetics by isothermal titration calorimetry." Curr Opin Struct Biol **11**(5): 560-566.

Li, A. Y., C. M. Stevens, B. Liang, K. Rayani, S. Little, J. Davis and G. F. Tibbits (2013). "Familial hypertrophic cardiomyopathy related cardiac troponin C L29Q mutation alters length-dependent activation and functional effects of phosphomimetic troponin I*." PLoS One **8**(11): e79363.

Li, M. X., L. Spyracopoulos and B. D. Sykes (1999). "Binding of cardiac troponin-I147-163 induces a structural opening in human cardiac troponin-C." Biochemistry **38**(26): 8289-8298.

Liang, B., F. Chung, Y. Qu, D. Pavlov, T. E. Gillis, S. B. Tikunova, J. P. Davis and G. F. Tibbits (2008). "Familial hypertrophic cardiomyopathy-related cardiac troponin C mutation L29Q affects Ca2+ binding and myofilament contractility." Physiol Genomics **33**(2): 257-266.

Lin, E., A. Ribeiro, W. Ding, L. Hove-Madsen, M. V. Sarunic, M. F. Beg and G. F. Tibbits (2014). "Optical mapping of the electrical activity of isolated adult zebrafish hearts: acute effects of temperature." Am J Physiol Regul Integr Comp Physiol.

McCubbin, W. D., M. T. Hincke and C. M. Kay (1980). "The effect of temperature on some calcium-binding properties of troponin C and calmodulin." Can J Biochem **58**(9): 683-691.

Moorman, A. F. and V. M. Christoffels (2003). "Cardiac chamber formation: development, genes, and evolution." Physiol Rev **83**(4): 1223-1267.

Moyes, C. D., T. Borgford, L. LeBlanc and G. F. Tibbits (1996). "Cloning and expression of salmon cardiac troponin C: titration of the low-affinity Ca(2+)-binding site using a tryptophan mutant." Biochemistry **35**(36): 11756-11762.

Negele, J. C., D. G. Dotson, W. Liu, H. L. Sweeney and J. A. Putkey (1992). "Mutation of the high affinity calcium binding sites in cardiac troponin C." J Biol Chem **267**(2): 825-831.

Nettleship, J. E., J. Brown, M. R. Groves and A. Geerlof (2008). "Methods for protein characterization by mass spectrometry, thermal shift (ThermoFluor) assay, and multiangle or static light scattering." Methods Mol Biol **426**: 299-318.

Olson, B. J. and J. Markwell (2007). "Assays for determination of protein concentration." Curr Protoc Pharmacol **Appendix 3**: 3A.

Ozdemir, S., V. Bito, P. Holemans, L. Vinet, J. J. Mercadier, A. Varro and K. R. Sipido (2008). "Pharmacological inhibition of na/ca exchange results in increased cellular Ca2+ load attributable to the predominance of forward mode block." Circ Res **102**(11): 1398-1405.

Parvatiyar, M. S., A. P. Landstrom, C. Figueiredo-Freitas, J. D. Potter, M. J. Ackerman and J. R. Pinto (2012). "A mutation in TNNC1-encoded cardiac troponin C, TNNC1-A31S, predisposes to hypertrophic cardiomyopathy and ventricular fibrillation." J Biol Chem **287**(38): 31845-31855.

Parvatiyar, M. S., J. R. Pinto, J. Liang and J. D. Potter (2010). "Predicting cardiomyopathic phenotypes by altering Ca2+ affinity of cardiac troponin C." J Biol Chem **285**(36): 27785-27797.

Pinto, J. R., M. S. Parvatiyar, M. A. Jones, J. Liang, M. J. Ackerman and J. D. Potter (2009). "A functional and structural study of troponin C mutations related to hypertrophic cardiomyopathy." J Biol Chem **284**(28): 19090-19100.

Putkey, J. A., W. Liu, X. Lin, S. Ahmed, M. Zhang, J. D. Potter and W. G. Kerrick (1997). "Fluorescent probes attached to Cys 35 or Cys 84 in cardiac troponin C are differentially sensitive to Ca(2+)-dependent events in vitro and in situ." Biochemistry **36**(4): 970-978.

Putkey, J. A., H. L. Sweeney and S. T. Campbell (1989). "Site-directed mutation of the trigger calcium-binding sites in cardiac troponin C." J Biol Chem **264**(21): 12370-12378.

Rarick, H. M., X. H. Tu, R. J. Solaro and A. F. Martin (1997). "The C terminus of cardiac troponin I is essential for full inhibitory activity and Ca2+ sensitivity of rat myofibrils." J Biol Chem **272**(43): 26887-26892.

Santer, R. M. (1974). "The organization of the sarcoplasmic reticulum in teleost ventricular myocardial cells." Cell Tissue Res **151**(3): 395-402.

Schmidtmann, A., C. Lindow, S. Villard, A. Heuser, A. Mugge, R. Gessner, C. Granier and K. Jaquet (2005). "Cardiac troponin C-L29Q, related to hypertrophic cardiomyopathy, hinders the transduction of the protein kinase A dependent phosphorylation signal from cardiac troponin I to C." FEBS J **272**(23): 6087-6097.

Schutte, D. P. and M. R. Essop (2001). "Clinical profile and outcome of idiopathic restrictive cardiomyopathy." Circulation **103**(14): E83.

Sia, S. K., M. X. Li, L. Spyracopoulos, S. M. Gagne, W. Liu, J. A. Putkey and B. D. Sykes (1997). "Structure of cardiac muscle troponin C unexpectedly reveals a closed regulatory domain." J Biol Chem **272**(29): 18216-18221.

Sievers, F., A. Wilm, D. Dineen, T. J. Gibson, K. Karplus, W. Li, R. Lopez, H. McWilliam, M. Remmert, J. Soding, J. D. Thompson and D. G. Higgins (2011). "Fast, scalable generation of high-quality protein multiple sequence alignments using Clustal Omega." Mol Syst Biol **7**: 539.

Skowronsky, R. A., M. Schroeter, T. Baxley, Y. Li, J. M. Chalovich and A. M. Spuches (2013). "Thermodynamics and molecular dynamics simulations of calcium binding to the regulatory site of human cardiac troponin C: evidence for communication with the structural calcium binding sites." J Biol Inorg Chem **18**(1): 49-58.

Sogah, V. M., F. C. Serluca, M. C. Fishman, D. L. Yelon, C. A. Macrae and J. D. Mably (2010). "Distinct troponin C isoform requirements in cardiac and skeletal muscle." Dev Dyn **239**(11): 3115-3123.

Spyracopoulos, L., M. X. Li, S. K. Sia, S. M. Gagne, M. Chandra, R. J. Solaro and B. D. Sykes (1997). "Calcium-induced structural transition in the regulatory domain of human cardiac troponin C." Biochemistry **36**(40): 12138-12146.

Stainier, D. Y., B. Fouquet, J. N. Chen, K. S. Warren, B. M. Weinstein, S. E. Meiler, M. A. Mohideen, S. C. Neuhauss, L. Solnica-Krezel, A. F. Schier, F. Zwartkruis, D. L. Stemple, J. Malicki, W. Driever and M. C. Fishman (1996). "Mutations affecting the formation and function of the cardiovascular system in the zebrafish embryo." Development **123**: 285-292.

Strynadka, N. C., M. Cherney, A. R. Sielecki, M. X. Li, L. B. Smillie and M. N. James (1997). "Structural details of a calcium-induced molecular switch: X-ray crystallographic analysis of the calcium-saturated N-terminal domain of troponin C at 1.75 A resolution." J Mol Biol **273**(1): 238-255.

Sweeney, H. L., R. M. Brito, P. R. Rosevear and J. A. Putkey (1990). "The low-affinity Ca2(+)-binding sites in cardiac/slow skeletal muscle troponin C perform distinct functions: site I alone cannot trigger contraction." Proc Natl Acad Sci U S A **87**(24): 9538-9542.

Takeda, S., A. Yamashita, K. Maeda and Y. Maeda (2003). "Structure of the core domain of human cardiac troponin in the Ca(2+)-saturated form." Nature **424**(6944): 35-41.

Talbot, J. A. and R. S. Hodges (1981). "Synthetic studies on the inhibitory region of rabbit skeletal troponin I. Relationship of amino acid sequence to biological activity." J Biol Chem **256**(6): 2798-2802.

Tardiff, J. C. (2011). "Thin filament mutations: developing an integrative approach to a complex disorder." Circ Res **108**(6): 765-782.

Tikunova, S. B. and J. P. Davis (2004). "Designing calcium-sensitizing mutations in the regulatory domain of cardiac troponin C." J Biol Chem **279**(34): 35341-35352.

Tripet, B., J. E. Van Eyk and R. S. Hodges (1997). "Mapping of a second actin-tropomyosin and a second troponin C binding site within the C terminus of troponin I, and their importance in the Ca2+-dependent regulation of muscle contraction." J Mol Biol **271**(5): 728-750.

Tsuda, S., A. Miura, S. M. Gagne, L. Spyracopoulos and B. D. Sykes (1999). "Low-temperature-induced structural changes in the Apo regulatory domain of skeletal muscle troponin C." Biochemistry **38**(18): 5693-5700.

Van Petegem, F. (2012). "Ryanodine receptors: structure and function." J Biol Chem **287**(38): 31624-31632.

Vogel, C. and E. M. Marcotte (2012). "Insights into the regulation of protein abundance from proteomic and transcriptomic analyses." Nat Rev Genet **13**(4): 227-232.

Vornanen, M. (1997). "Sarcolemmal Ca influx through L-type Ca channels in ventricular myocytes of a teleost fish." Am J Physiol **272**(5 Pt 2): R1432-1440.

Vornanen, M. (1998). "L-type Ca2+ current in fish cardiac myocytes: effects of thermal acclimation and beta-adrenergic stimulation." J Exp Biol **201**(Pt 4): 533-547.

Vornanen, M., H. A. Shiels and A. P. Farrell (2002). "Plasticity of excitation-contraction coupling in fish cardiac myocytes." Comp Biochem Physiol A Mol Integr Physiol **132**(4): 827-846.

Wang, D., I. M. Robertson, M. X. Li, M. E. McCully, M. L. Crane, Z. Luo, A. Y. Tu, V. Daggett, B. D. Sykes and M. Regnier (2012). "Structural and functional consequences of the cardiac troponin C L48Q Ca(2+)-sensitizing mutation." Biochemistry **51**(22): 4473-4487.

Willott, R. H., A. V. Gomes, A. N. Chang, M. S. Parvatiyar, J. R. Pinto and J. D. Potter (2010). "Mutations in Troponin that cause HCM, DCM AND RCM: what can we learn about thin filament function?" J Mol Cell Cardiol **48**(5): 882-892.

Wiseman, T., S. Williston, J. F. Brandts and L. N. Lin (1989). "Rapid measurement of binding constants and heats of binding using a new titration calorimeter." Anal Biochem **179**(1): 131-137.

Zhang, P. C., A. Llach, X. Y. Sheng, L. Hove-Madsen and G. F. Tibbits (2011). "Calcium handling in zebrafish ventricular myocytes." Am J Physiol Regul Integr Comp Physiol **300**(1): R56-66.